Genetic Interactions and Biochemical Pathway Involved in Escape from *het-6* Incompatibility in *Neurospora crassa*

by

Ghazaleh Nourparvar

A thesis submitted to the Faculty of Graduate and Postdoctoral Affairs in partial fulfillment of the requirements for the degree of

Master of Science

in

Biology

Carleton University
Ottawa, Ontario

Abstract

Non-self recognition during asexual growth in filamentous fungi is mediated by interactions between proteins encoded by heterokaryon incompatibility (*het*) genes. For example, *N. crassa* strains that carry the incompatible factors *un-24*^{PA} and *het-6*^{OR} exhibit a slow and aberrant growth phenotype. *un-24* encodes for the large subunit of ribonucleotide reductase (RNR) and its C-terminus is involved in incompatibility. To date, the only function assigned to *het-6* is incompatibility. Remarkably, after about 4.5 days of growth, wild-type-like sectors emerge from these self-incompatible *un-24*^{PA} *het-6*^{OR} colonies through a process called 'escape'. Escape is due to point mutations that arise in *het-6* gene (94%), *vib-1* (3%), a transcription factor of *het-6*, or other factor(s) (3%) that have only been characterized by a unique feathery morphology. To investigate the mechanism of escape we separately introgressed into *un-24*^{PA} *het-6*^{OR} strains each of 80 gene mutations including deletions of genes encoding low-fidelity DNA polymerases and DNA repair factors, and tested whether these mutations suppress escape. Results show that deletions of the DNA damage checkpoint factors, *mus-9*, *uvs-3, mus-23* (orthologs to human ATR, ATRIP and MRE11 respectively), *vib-1* and *rtt109* (H3K56 acetyltransferase which is more abundant in *N. crassa* treated with hydroxyurea) either suppress or delay escape from incompatibility. Preliminary RT-qPCR data suggests that within 1 hour, there is 7 and 3.5 fold change in expression of *het-6* and *vib-1*, respectively, when RNR is inactivated by addition of hydroxyurea. We proposed that *het-6* and *vib-1* are DNA damage checkpoint effectors.

Acknowledgements

First and foremost I want to thank my supervisor Dr. Myron Smith. I sincerely appreciate your support and guidance throughout my research. You always kept me enthusiastic through the ups and downs. I also want to take this time to thank my advisory committee Dr. Hepworth, Dr. Lambert and Dr. McKay for their help and invaluable suggestions to grow my research. I thank Dr. Linda Bonen and Dr. Tim Xing for being part of my defense committee. I would also like to thank Darlene Moss for all her help and kindness.

I want to acknowledge all Smith lab members for their friendship and help: Bodunde, Ghyda, Abi, Leena, Imelda, Jessica, Iryna, Emma and Mustafa. I am especially grateful to Ryan Reshke for teaching me how things go in Smith lab, Denis Lafontaine for generously sharing his knowledge of incompatibility and escape and Anatoly Belov for answering my many questions.

I am very appreciative to my family, especially my sisters, who have always encouraged me to follow my dreams.

Last but not least, I want to thank my husband for his unconditional love and support and listening to me talking about fungi and escape days and nights.

Table of Contents

List of Tables

List of Figures

List of Abbreviations

°C	degree Celsius
DDR	DNA damage response
dNTP	deoxyribonucleotide diphosphate
DSB	double stranded break
HI	heterokaryon incompatibility
hph	hygromycin phosphotransferase
HR	homologous recombination
HU	hydroxyurea
MHC	major histocampatibility complex
mm	millimeter
mM	millimolar
MMS	methyl methanesulfonate
NDP	ribonucleotide diphosphate
NHEJ	non-homologous end joining
OR	Oak Ridge
PA	Panama
PCD	programmed cell death
RNR	large subunit of ribonucleotide reductase
RT-qPCR	reverse transcriptase quantitative PCR
SCM	synthetic crossing medium
SI	self incompatible
SSB	single stranded break
UV	ultra violet
vic	vegetative incompatibility
VMM	Vogel's minimum medium
WT	wild type
µm	micrometer

List of Appendices

Introduction

Non-self recognition: Non-self recognition systems have evolved in almost all organisms from prokaryotes to eukaryotes. In bacteria, as prokaryotes, restriction enzyme systems govern recognition of exploitive DNA (Tock and Dryden, 2005). In eukaryotes, non-self recognition systems include polymorphic loci under diversifying selection. From plants (Charlsworth *et al*., 2005) to vertebrates, these loci are composed of tightly linked genes with reduced recombination ability to prevent disruption of adaptive gene complexes (reviewed in Nasrallah, 2002; Nasrallah, 2005). In vertebrates, the major histocompatibility complex (MHC) system encodes for groups of proteins involved in immune response (Kumanovics *et al.,* 2003). These systems also contain polymorphic loci under balancing selection. Similar to other eukaryotic cells, the ability to distinguish self from non-self evolved in filamentous fungi such as *Neurospora crassa* and is controlled by polymorphic loci. These loci regulate hyphal fusion and heterokaryon formation during vegetative growth.

Fungal heterokaryon incompatibility: In filamentous fungi, non-self recognition systems that operate during vegetative growth are controlled by heterokaryon incompatibility loci (*het* loci). During vegetative (asexual) growth of filamentous fungi, hyphae from genetically dissimilar individuals of the same species can fuse together to result in a 'heterokaryon'. A heterokaryon consists of two or more nuclei carrying different genetic makeup that share the same cytoplasm. Heterokaryon formation can be beneficial since the different nuclei may be able to confer novel resistance combinations and complement each other's deficiencies (Glass *et al*., 2000).

In any given filamentous fungus species there are 5-20 *het* loci which modulate hyphal fusions; combining two nuclei that differ at one or more *het* loci will result in slow aberrant growth or programmed cell death. This is usually referred to as "vegetative incompatibility (vic)" or "heterokaryon incompatibility (HI)". HI systems may reduce the risk of being overtaken by aggressive genotypes and transmission of infectious mycoviruses and plasmids (Debets *et al*., 1994; Debets and Griffiths*,* 1998; Biella *et al*., 2002). HI systems have only been most the thoroughly investigated in the species *Neurospora crassa, Podospora anserina* and *Cryphonectria parasitica*.

To date, the unified characteristics of fungal HI systems are a) incompatibility loci comprise a gene complex, b) one of the genes in the complex encodes a 'HET' domain, and c) there is a non-allelic interaction between a HET-domain-encoding gene and another gene, which usually encodes for a protein that has a function in addition to HI. The HET domain (PFAM06985) comprises three conserved regions that are found in the predicted products of HI genes such as *het-6*, *tol* and *pin-c* in *N. crassa*, *het-d* and *het-e* in *P. anserine*, and *vic6* and *vic7* of *C. parasitica* (Smith and Lafontaine, 2012) (Figure 1). Ultimately, the presence of various incompatibility gene combinations in the same cytoplasm triggers HI. For example, *het-c* gene in *P. anserina* is a putative glycolipid transfer protein. Non-allelic interaction between *het-c* and either HET domain gene *het-e* or *het-d* promotes HI (Espagne *et al.,* 2002). In *N. crassa*, *het-c pin-c* incompatible combinations initiate HI response; the *het-c* gene encodes a putative plasma membrane protein and the closely linked *pin-c* gene encodes a HET domain protein (Kaneko *et al.,* 2006). *tol* is another HET domain gene and it modulates incompatibility that initiates by interaction of MAT-A and MAT-a during vegetative growth of *N. crassa* strains.

***het-6* locus**: In *Neurospora crassa* two tightly linked genes, *het-6* and *un-24*, comprise the *het-6* locus (Smith *et al.,* 2000). Two allelic variants of these genes, Panama (PA) and Oak Ridge (OR), are in severe linkage disequilibrium to the extent that only *un-24*^{PA} *het-6*^{PA} and *un-24*^{OR} *het-6*^{OR} haplotypes are found in nature (Mir-Rashed *et al.,* 2000). Any other combinations result in incompatibility reactions (Micali and Smith, 2006) (Figure 2). There is extreme divergence between DNA sequences in the region between *un-24* and *het-6* when the two haplotypes are compared due to a paracentric inversion break point (Figure 3). This sequence dissimilarity prevents any homologous recombination between the two morphs and contributes to their linkage disequilibrium (Micali and Smith, 2006).

Similar to other fungal incompatibility loci, the *het-6* gene in the *het-6* locus encodes a protein with a HET domain. The *het-6* OR and PA morphs share only 78% identity at the nucleic acid level and 68% identity at the amino acid level. To date, other than incompatibility, no other function is attributed to the HET-6 protein product (Micali and Smith, 2006).

The *un-24* gene encodes the large subunit of a Type I ribonucleotide reductase (RNR), which is an evolutionary conserved protein that is necessary for *de novo* deoxyribonucleotide synthesis (Jordan & Reichard, 1998). In Type I RNRs, two large subunits and two small subunits form a tetramer protein complex that catalyzes the reduction of ribonucleoside diphosphates (NDPs) to deoxyribonucleoside diphosphates (dNDPs). Further phosphorylation of the dNDPs to dNTPs provides the building blocks of DNA synthesis (Jordan & Reichard, 1998). Formation of thiyl radicals is essential for the conversion of corresponding NDPs to dNDPs. The RNR small subunit interacts with

a diferric centre in presence of oxygen and generates a thyrosyl radical that is transferred to the active catalytic site in the large subunit. The large subunit also contains two allosteric control sites that control activity and specificity of the holoenzyme (Reichard, 2001). Balanced pools of dNTPs are essential during cell growth and mitosis to maintain the integrity of DNA. Any alterations in the concentration of the available dNTPs may result in stalled replication forks and/or incorporation of wrong nucleic acids into newly synthesized DNA (Buckland *et al*., 2014).

In *N. crassa*, co-expressing of *un-24*^{OR} and *un-24*^{PA} results in a weak incompatibility reaction (Smith *et al*., 2000). The N-terminal coding sequence in *un-24* is highly conserved and it was shown to not be involved in incompatibility; however, the two morphs are highly divergent in the C-terminus region where incompatibility activity and specificity is localized (Smith *et al*., 2013). In the tetramer complex, the C-terminus of one large subunit monomer is responsible to reduce the catalytic site of the other large subunit. The model proposed by Smith *et al*. (2013) is that during interaction of the C-terminus and catalytic site, OR and PA forms of UN-24 become covalently linked and inactivated. Interestingly, it has also been found that changing one glutamic acid residue in the C-terminus of UN-24^{OR} to leucine results in a null allele that is compatible with both OR and PA haplotype (Reshke, 2013). That one single amino acid alteration can govern recognition of self from non-self in an organism is amazing.

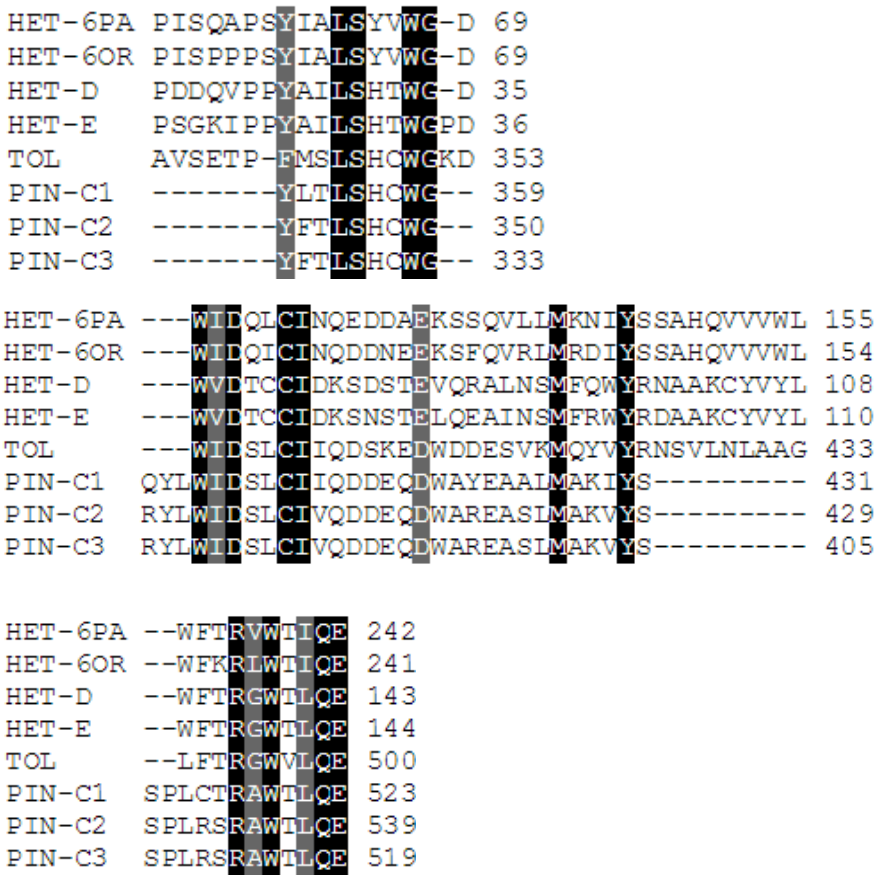

Figure1. Alignment of the three conserved regions that make up the HET domain in six HI protein products using MUSCLE. HET-6^{OR}, HET-6^{PA}, TOL, PIN-C1, PIN-C2 and PIN-C3 (Accession numbers are: AF206700, AF208542, AF085183, HQ396391, HQ396394.1 and HQ396333.1, respectively) are found in *Neurospora crassa*. HET-D and HET-E (Accession numbers are AF323585 and L28125, respectively) are found in *Podospora anserina*. Each block shows one conserved region. Black background shows identical amino acids among all sequences. Gray background shows amino acids with similar R-groups. White background shows dissimilar amino acids. Numbers indicate the last amino acid in the conserved region.

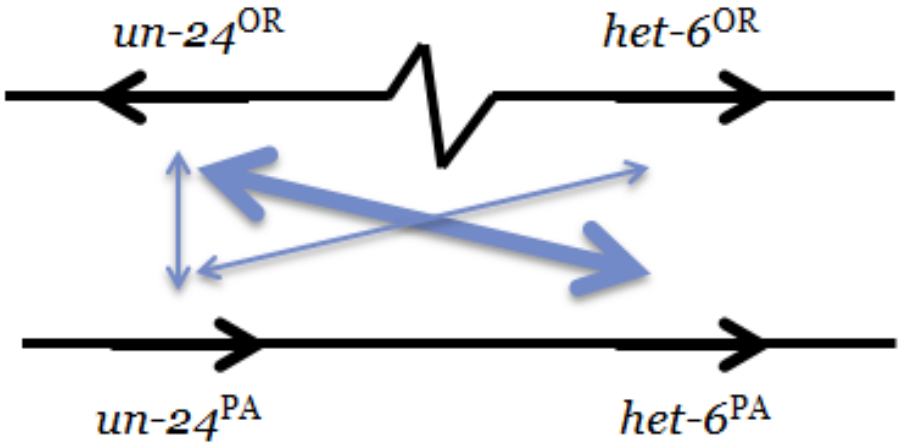

Figure 2. Allelic and non-allelic interactions of *het-6* locus. Black arrows indicate the genes. Blue arrows represent incompatibility interactions. Thick blue arrow shows severe non-allelic incompatibility between $un\text{-}24^{OR}$ and $het\text{-}6^{PA}$. Thin blue arrows show milder allelic incompatibility between $un\text{-}24^{OR}$ and $un\text{-}24^{PA}$, and non-allelic incompatibility between $un\text{-}24^{OR}$ and $het\text{-}6^{PA}$. Figure adapted from Lafontaine and Smith (2012).

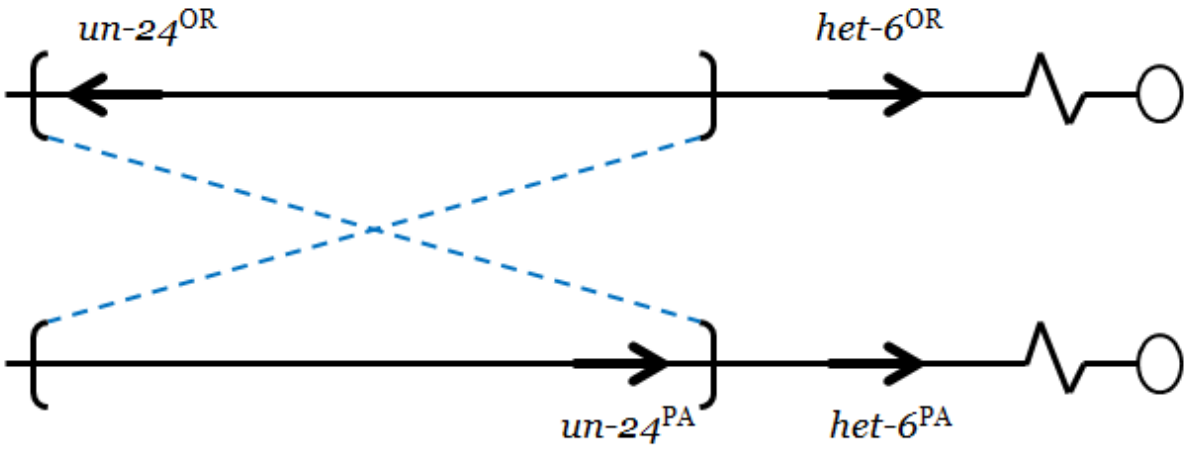

Figure 3. DNA sequence alignment of Oak Ridge and Panama haplotypes of *het-6* locus reveal sequence divergence at the right paracentric inversion break point (represented by parenthesis) within the left arm of linkage group II (circles indicate the centromeres). Genes are represented by black arrows. Figure is adapted from Micali and Smith (2006).

Escape: "Escape" from heterokaryon incompatibility happens during vegetative growth when slow growing self-incompatible fungal strains spontaneously change to a wild-type growth rate and phenotype. An early attempt to understand escape from *het-6* incompatibility employed translocation partial diploids (Smith *et al.,* 1996). In this case, escape was associated preliminary with deletion of the ectopic (OR) haplotype, whereupon the slow-growing SI colony converted to a wild-type growth rate and phenotype. Allele inactivation happened due to large deletions some of which were several hundred kbp (Smith *et al*., 1996).

Escape has also been previously studied in *Podospora anserina* self-incompatible transformants. *het-R het-V* or *het-C het-E* self-incompatibility was suppressed by mutations in *het-R* but not *het-V* or *het-E* but not *het-C*. Both *het-R* and *het-E* belong to the *hnwd* gene family with WD-repeat domains. Mutations in *het-R* and *het-E* associated with escape include deletions, duplications and modifications in the number of WD-repeats that change the incompatibility specificity of the strains. Finding mutations in *hnwd* genes, and not the other *het* gene, suggested genetic instability is specifically associated with these *hnwd* loci (Chevanne *et al.,* 2010).

In the *het-6* locus, the allelic interaction between *un-24*^{OR} and *un-24*^{PA} has been studied in strains deleted for *het-6* (Lafontaine and Smith, 2012). The allelic incompatibility associated with *un-24* is weak, with only ~50% growth rate reduction, and escape occurs by an unknown process within about 2 days. Non-allelic incompatibility between *un-24*^{OR} and *het-6*^{PA} or between *un-24*^{PA} and *het-6*^{OR} are severe and asymmetrical (Micali and Smith, 2006). For example transformation of *un-24*^{OR} into *het-6*^{PA} strains results in a complete loss of viability. In contrast, transformation of *un-*

24^{PA} into a *het-6*^{OR} strain results in colonies that grow slowly and with a 'star-like' morphology. These *un-24*^{PA} *het-6*^{OR} SI transformants escape to a wild-type phenotype within 4-7 days (Micali and Smith, 2006). How the fungus maintains its genetic integrity and manages to inactivate the right gene in order to restore the wild-type form is unknown, but the process is reminiscent of directed mutations in other systems.

The best example of a system that resembles escape is hypermutation in B-cells in mammalian system. Germinal center B cells are the core of the human adaptive immune system and they present antibody on their surfaces. Upon antigen binding, B-cells start proliferation which is accompanied by a high rate of base substitution in the hypermutable region of antibody gene. This leads to daughter B-cells that present slightly different surface antibodies, some of which bind better to the antigen and thus outcompete other B-cells. This results in evolution of B-cells that provide antibodies with increasingly improved antigen binding (Zan and Casali, 2015). They leave germinal centers as memory B-cells while others undergo programmed cell death (MacLennan, 1994). However, to maintain the appropriate mutations in the immunoglobulin loci, DNA damage checkpoints have to be turned off during the latter process in the centroblasts. Therefore, ATR/Chk1 pathway is suppressed by upregulation of transcriptional respressor Bcl-6 (Ranuncolo *et al*., 2008). Bcl-6 is a zinc finger transcription factor and is a sequence specific suppressor of transcription involved in B cell immune response. Bcl-6 upregulation suppresses all members of the ATR/Chk1/p53 damage response and as a result B- cells will be able to undergo hypermutation in an error prone mode while the rest of the DNA material is transcribed in a high fidelity manner. DNA damage

checkpoints will be discussed in more details in the coming paragraphs since they appear to play a role in escape from *het-6* incompatibility in *N. crassa* as well.

HI suppressors: To date, two suppressors of HI in *N. crassa* have been identified. First, the *tol* gene, which encodes a HET-domain protein, is required for vegetative incompatibility associated with mating type (Vellani *et al*., 1994; Leslie & Yamashiro, 1997). For successful mating in *N. crassa*, fusion of hyphae carrying different mating type is essential. However, during vegetative growth, fusion of such hyphae results in incompatibility and leads to growth inhibition and cell death. A functional *tol* gene is required for this process since mutations in *tol* completely abolishes *mat*-associated vegetative incompatibility.

Second, mutations in the *vib-1* locus of *N. crassa* were discovered that suppress *het-c* incompatibility (Xiang and Glass 2002; Xiang and Glass 2004; Dementhon *et al*., 2006). VIB-1 is one of three homologues in *N. crassa* of transcription factor Ndt80p from *Saccharomyces cerevisiae*. Ndt80p is involved in regulation of meiosis in yeast. Mutations in NDT80 result in arrest of the meiotic cell cycle at pachytene (Xu *et al.,* 1995). It has also been proposed that Ndt80p is only activated when meiotic pachytene checkpoint signal is off (Hepworth *et al*., 1998). Therefore, it seems that Ndt80p is controlled by a RAD17-dependent checkpoint. RAD17 in *S. cerevisiae* is homologue of human Rad1 and it activates the DNA damage and meiotic pachytene checkpoint.

VIB-1 is a putative transcription factor and it has a predicted DNA binding domain and nuclear localizing sequence that are similar to those in Ndt80p. VIB-1 is required for the transcription of *het-6* (Figure 4), *pin-c* and *tol* (Dementhon *et al.,* 2006;

Lafontaine and Smith, 2012). VIB-1 is predicted computationally to have one binding domain upstream *het-6*^{OR} and two binding domains upstream *het-6*^{PA}. Interestingly, it has been shown that *vib-1*$^{-}$ strains have lower levels of *het-6*^{OR} expressed than do *vib-1*$^{+}$. In contrast, *het-6*^{PA} is moderately upregulated in *vib-1*$^{-}$ strains (Lafontaine and Smith, 2012). VIB-1 is known to be differentially localized during the asexual cell cycle and HI of *N. crassa*. During the sexual cycle of wild-type strains, VIB-1 is localized to mature conidia. However, during PCD from HI, it is localized to live cells surrounding the dying cells (Dementhon *et al*., 2006). In *N. crassa*, VIB-1 is also involved in secretion of extracellular protease in response to carbon and nitrogen starvation (Dementhon *et al.,* 2006). These associations indicate that there may be a link between starvation, cell death and HI mediated by VIB-1. All known VIB-1 functions are summarized in Figure 4. The other two homologues of NDT80 (NCU09915 and NCU04729) have not been associated with HI and asexual cycle.

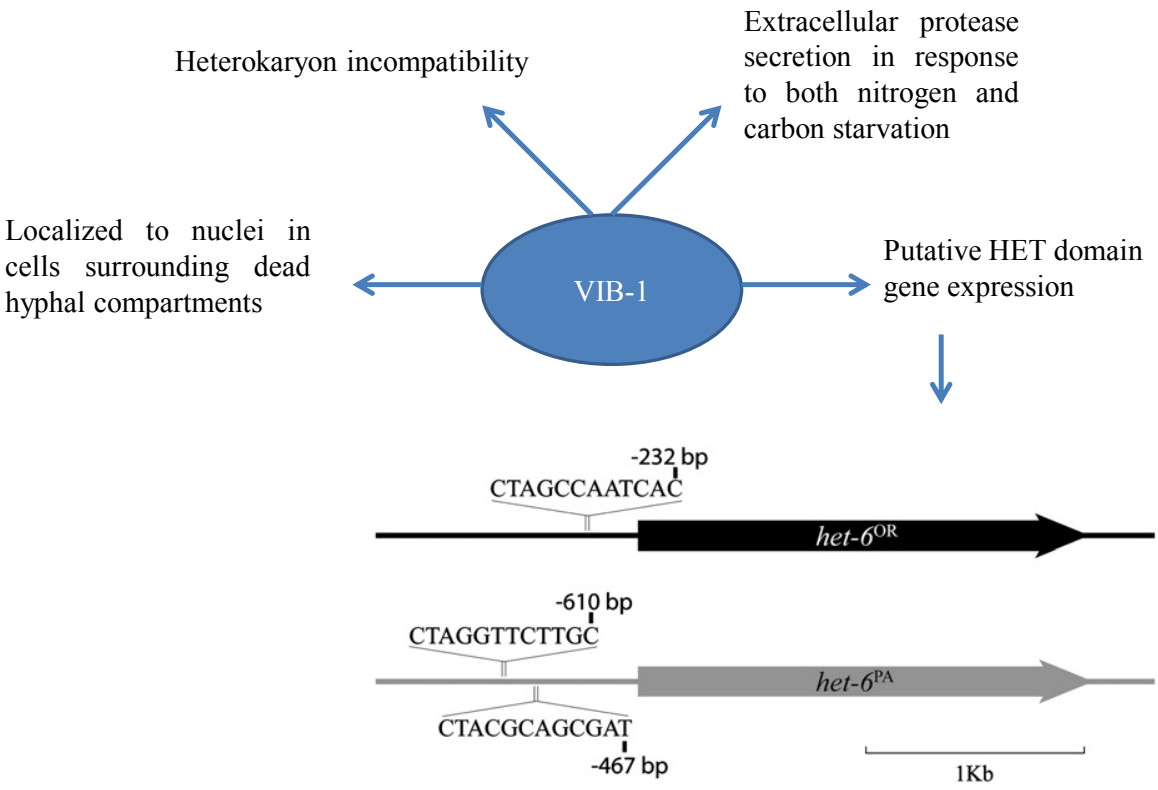

Figure 4. Schematic of various VIB-1 functions. Figure is adapted from Dementhon *et al.* (2006) and Lafontaine and Smith (2012).

Genome stability and DNA damage response

In this study, we explore escape from heterokaryon incompatibility in *un-24*^{PA}*het-6*^{OR} strains. We show that escape from *un-24*^{PA} *het-6*^{OR} incompatibility results in mutation of either *het-6* or *vib-1* and that this process occurs in a very predictable manner. We also explore the timing and behavior of escape in cells that carry knock-out mutations of genes that are associated with genome stability.

Genome stability is an integral process in the cell to ensure accurate transfer of hereditary material through the generations. External factors such as exposure to UV and certain chemicals and internal factors such as reactive oxygen species can cause replication errors (Zeman and Cimprich, 2014). DNA damage includes any changes in the base or nucleotides or a break in the DNA backbone. Damage to the DNA can stop polymerase during replication and result in single or double stranded breaks (SSB and DSB respectively). To ensure genetic information passed on to daughter cells is accurate, several signaling and checkpoint processes act together or in a redundant manner upstream of DNA damage response (DDR) to sense any DNA damage during the cell cycle and to ensure that the original DNA information is restored to the maximum extent prior to replication. DNA damage checkpoint proteins are able to manipulate cell cycle progression and activate DNA repair. Subsequently, DNA repair can be achieved by two main mechanisms: homologous recombination (HR) or non-homologous end-joining (NHEJ) (Ciccia and Elledge, 2010; Bartek and Lucas, 2007).

DNA damage proteins are categorized into damage sensors, transducers and effectors. Once damage is detected by sensors, a signal is transduced to effectors which, in turn, are able to instigate the appropriate action of either suspending the cell cycle and triggering cell death or recruiting DNA repair proteins. DNA damage checkpoints are evolutionarily highly conserved and are well-studied in *Saccharomyces cerevisiae* and human cells.

The central components of DNA damage response transduction are phosphatidylinositol 3-kinases (PI3) which through cascades of chemical modifications sense and repair various types of breaks in DNA. In human cells, two main mediators of DNA damage response belonging to PI3 family are Ataxia Telangiectasia Rad3 Related (ATR) and Ataxia Telangiectasia Mutated (ATM) genes.

ATR and its regulatory protein ATRIP are clamped to the site of DNA damage at stalled replication forks coated with replication protein A (RPA). RPA coated ssDNA also loads 9-1-1 heterodimer (RAD9- RAD1-HUS1) to promote ATR kinase activity. The damage signal is then amplified by phosphorylation of effectors either by ATR/ATRIP itself or other kinases such as ChK1 protein. In this case the repair system activated is usually the error-free homologous recombination (Zeman and Cimprich, 2014; Marechal and Zou, 2013).

ATM, on the other hand, is recruited to the site of DSBs by MRN complex which includes MRE11-RAD50-NBS1. Association of the NBS-1 C-terminus with ATM is crucial for recruitment of ATM to the site of damage. Each member of the complex is then phosphorylated by ATM to act as adaptors to control checkpoint activity and

mediate DNA repair and cell survival (Lavin *et al*., 2015). The effectors can also be phosphorylayed by ATM itself or by other kinases such as ChK2. ATM checkpoint pathway is usually resulted in error-prone DNA repair especially NHEJ (Marechal and Zou, 2013).

In DNA damage response systems, the cascade of phosphorylations promotes various cellular activities of effectors that are important for maintaining genome stability. These cellular responses range from cell cycle arrest and apoptosis to DNA repair (Boiteux and Robertson, 2013). One of these effectors in mammalian cells is p53, a transcription factor important both for activation and suppression of transcription of genes involved in DNA repair, development, autophagy and metabolism. p53 is the critical hub of a highly branched pathway that receives signals from an array of cellular functions and then, based on these signals and the current cell condition, it may activate various cell responses. p53 can receive signals related to DNA damage, DNA replication stress and imbalances in the dNTP pools. It then can activate cell functions such as DNA repair, cell cycle arrest, apoptosis and changes in cell metabolism (Mantovani *et al.,* 2015). p53 has been found only in metazoan (Belyi *et al*., 2012). However, because the function of p53 is very complex and critical for cell processes, orthologous counterparts must occur in other taxa, including plants and fungi. Some of the functions of p53 are presented in Figure 5.

There are many similarities and differences in the DNA damage response factors in *N. crassa*, yeast and mammalian cells (Table 1). Mec1 and Tel1 are the main components of DNA damage response in *S. cerevisiae,* and have their respective orthologues ATR and ATM in mammalian cells (Zou, 2013).

The orthologue of the mammalian 9-1-1 complex in *S. cerevisiae* is a complex that contains Ddc1, Rad17 and Mec3. When clamped to the site of DNA damage this Ddc1/Rad17/Mec3 complex is both necessary and sufficient to activate the Mec1 dependent checkpoint (Majka *et al*., 2006). The orthologue of the MRN complex in *S. cerevisiae* is designated as MRX (Mre11, Rad50 and Xrs2). Although MRX plays a crucial role in NHEJ in yeast, MRN does not play a significant role in NHEJ in mammalian cells (Leiber, 2010). It is suggested that Mec1 plays the major role in any DNA damage signaling pathway in yeast. Tel1 is only activated when Mec1 is absent (Sanchez *et al.,* 1996). In contrast, ATM is essential in healthy mammalian cells and any mutations in this gene can lead to severe conditions such as ataxia telangiectasia. This shows that although these pathways are evolutionary conserved in various organisms, the way they function may differ in different organisms.

DNA damage checkpoints in *N. crassa*: In *Neurospora crassa*, it is found that the mutagen sensitive group of *mus-9* and *uvs-3* are functionally similar to human ATR and ATRIP respectively (Kazama *et al.,* 2007). MMS and UV sensitivities of strains with mutations in *uvs-3* are compensated by plasmids containing *uvsD*, the *Aspergillus* orthologue of ATRIP. On average, conidia from *uvs-3* mutant strains have 6% more micronuclei compared to wild-type. Also, germination in the presence of 0.1M hydroxyurea, an inhibitor of RNR and thus DNA replication, increased from 10.7% in wild-type to 50% in the *uvs-3* mutant strain. All of this suggests cell cycle deficiency and a role for *uvs-3* in DNA damage checkpoint function. Although there is little sequence similarity between *uvs-3* in *N. crassa* and other orthologues of ATRIP in other organisms, a coiled-coil structure is predicted at the N-terminal of the UVS-3 which is

important for its function. In *S. pombe*, *rad26* is the orthologue of *uvs-3* in *N. crassa*. RAD26 protein interacts with RAD3. The closest *rad3* orthologue is *mus-9* in *N. crassa* and it is the functional homologue of human ATR. Northern blot analysis showed both *uvs-3* and *mus-9* mRNA levels increased after UV exposure.

Homology analysis identified four genes of *mus-21*, *mus-58*, *mus-59* and *prd-4* that may be implicated in cell cycle control. *mus-21* is the orthologue of mammalian ATM and homologue of Tel1 in yeast. *mus-58* is the orthologue of mammalian CHK1 and *mus-59* and *prd-4* are two orthologues of mammalian CHK2. However, their interactions are different from those found in mammalian cells. Experiments had shown an epistatic relationship between *mus-9/mus-58* and *mus-21/prd-4*. However, *mus-9/mus-59* and *mus-21/mus-58* double mutants showed reduced sensitivity to mutagens (Wakabayashi *et al.,* 2008). These results suggest that both *mus-9* and *mus-21* are interacting with *mus-58* and *mus-59*. Therefore, it seems clear that Mec1/Chk1 and Tel1/Chk2 interactions in yeast are not conserved for homologous *N. crassa* checkpoint proteins.

The MRX/MRN complex is studied in *N. crassa* (Watanabe *et al.,* 1997). The *mus-23* gene is an orthologue of *mre-11* and its mutants are defective in recombinational repair. The other two proteins of this complex, *uvs-6* and *nbs-1* are not well studied in *N. crassa*. However, based on homology, NBS-1 and UVS-6 are orthologues of human NBS-1 and RAD-50, respectively. It is not known whether three proteins interact in a complex to recruit *mus-21* to the site of damage, as is the case in mammalian and yeast systems.

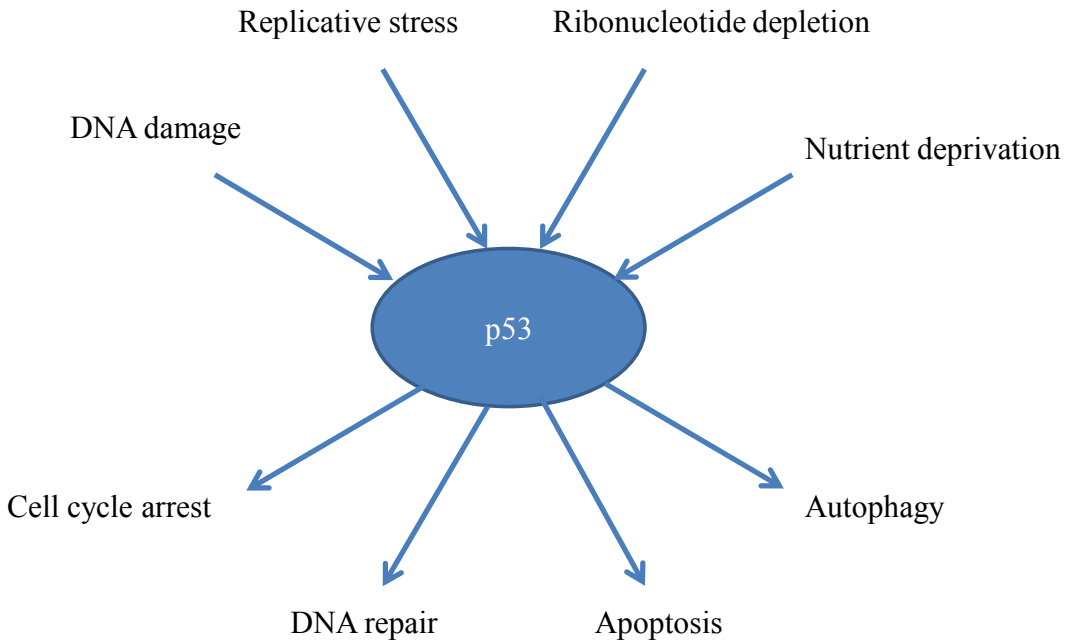

Figure 5. Summary of p53 functions in mammalian cell. p53 is a transcription factor and an important effector of DNA damage checkpoint. Various cellular signals are able to activate p53. Upon activation p53 can mediate various responses in the cell. Figure is adapted from Mantovani *et al.* (2015).

Table 1. DNA damage checkpoint factors in human, *S. cerevisiae* and *N. crassa.* Proteins at each row are found to have similar functions. For Expect values of homology check Appendix A.

Human	*S. cerevisiae*	*N. crassa*
ATR	Mec1	*mus-9*
ATRIP	Ddc2	*uvs-3*
CHK1	Chk1	*mus-58*
ATM	Tel1	*mus-21*
CHK2	Rad53	*mus-59, prd-4*
MRN/MRX complex		
MRE11	Mre11	*mus-23*
RAD50	Rad50	*uvs-6* (heterokaryon)
NBS1	Xrs2	*nbs-1*
9-1-1 complex		
RAD9	Ddc1	unknown
RAD1	Rad17	unknown
HUS1	Mec3	unknown

Interestingly, here we report a process in *Neurospora crassa* where *mus-9*/*uvs-3* DNA damage checkpoint is involved in directing a point mutation to specific loci in order to resume growth stalled by heterokaryon incompatibility and restore maximum DNA stability possible for the next generation through 'escape'.

Objective

The objective of my M.Sc. research is to investigate genetic interactions and biochemical pathways involved in escape from *het-6* associated heterokaryon incompatibility. To carry out the research, I used the strain *un-24*^{PA} *het-6*^{OR} (Lafontaine and Smith, 2012). This strain was synthesized by homologous replacement of a temperature sensitive allele of *un-24*^{OR} with *un-24*^{PA}. The resulting *un-24*^{PA} *het-6*^{OR} strain was self-incompatible (SI). It mimics a heterokaryon that has *un-24*^{PA}*het-6*^{PA} and *un-24*^{OR}*het-6*^{OR} nuclei sharing the same cytoplasm. To keep the strain in pre-escape genotype, a mutation in the *vib-1* locus was introgressed into the *un-24*^{PA} *het-6*^{OR}. *vib-1* partially suppresses the *un-24*^{PA} *het-6*^{OR} incompatibility phenotype and blocks escape. To investigate the effect of each gene deletions on escape behavior, the *un-24*^{PA} *het-6*^{OR}; *vib-1* strain was crossed with other OR strains that bear a specific knockout of a gene of interest. For a source of gene deletions, I used the *Neurospora crassa* gene knockout library available through the Fungal Genetics Stock Center (FGSC, University of Kansas Medical Center). After crossing, I selected progeny that were genotypically *un-24*^{PA} *het-6*^{OR} ΔXXX, where ΔXXX designates a gene deletion. I was able to closely monitor the timing and phenotype of pre- and post-escape colonies. These results were then used to propose a model of genetic interactions in dissecting the escape process.

Methods

Strains, culture and cross conditions:

All *N. crassa* strains were cultured on Vogel's Minimum Medum (VMM) with 1.5% sucrose, 1.5% agar, and other required supplements (Davis and De Serres, 1970). Cultures were grown in a dark incubator at 30°C unless stated otherwise. Strains used for crossing, microscopy and RNA extraction are listed in Table 2. Strains with gene knockouts are listed in Appendix A.

All *N. crassa* crosses were performed on plates containing Synthetic Crossing Medium (SCM) with required supplements (Davis and De Serres, 1970). Conidial or mycelia suspensions of opposite mating-type strains were spotted at opposite edges of the plate. Cultures were allowed to grow at room temperature (21°C to 25°C) under natural light until perithecia with ascospores were formed.

Spot tests were performed to test for hygromycin resistance by inoculation of conidial or mycelial suspensions of strains on slants containing VMM with supplements and 4 mg of hygromycin B (Roche, Laval, Canada) per 100ml of medium.

Microscopy and imaging:

For scanning electron microscopy (SEM), strains were grown on permeable membranes overlaid on top of VMM with required supplements in 30°C. Wild-type and Type I strains were grown for 12 hours, Type II and Type III escapes were grown for 24 hours and SI strains were grown for 72 hours prior to microscopy. SEM was done in the

Nano Imaging Facility (Carleton University) following gold plating of samples. Hyphal diameter and branch angles were measured using Adobe Photoshop CS5.

For fluorescent microscopy, *N. crassa* strains were cultured on slides that were previously dipped into VMM with required supplements. Conidial or mycelial suspensions were spotted on the slide and allowed to grow in a moist chamber at room temperature under natural light. A moist chamber consists of a glass Petri dish with a moist filter paper at the bottom housing the slide (Figure 6). Wild-type and Type I escape strains were grown for 12 hours, Type II and Type III escape strains were grown for 24 hours and SI strains were grown for 48 hours prior to microscopy. The cells were then fixed with 70% ethanol or left untreated and then stained with 0.05% DAPI to count the nuclei per cell (Raju, 1982) using a fluorescent microscope (Zeiss Axioplan2 imaging, Zeiss AxioCam HRc camera) to see blue signals from the stained nuclei.

Table 2. Strains used in this study.

Strain[1]	Genotype	Origin
Strains used for crosses		
DLL-14(6)	*un-24*^{PA}*het-6*^{OR}*; vib-1*$^{-}$ *inl A*	ML Smith
DLL-T2K(0)	*un-24*^{PA}*het-6*^{OR}*; vib-1*$^{-}$ *inl a*	ML Smith
C9-2 :: *un* ^{PA} (control)	*un-24*^{PA}*het-6*^{OR}*; thr-2 a*	ML Smith
DLL-T4a	*un-24*^{OR}*het-6*^{OR}*; Δmus-9 a*	ML Smith
qde-2	*un-24*^{OR}*het-6*^{OR}*; Δqde-2 a*	ML Smith
Ku70	*un-24*^{OR}*het-6*^{OR}*; Δmus-51 a*	ML Smith
Strains used for microscopy		
Type I escape[2]	*un-24*^{PA}*het-6*^{OR*}[3]	DLL-T2K(0) x FGSC12048
Type II escape[2]	*un-24*^{PA}*het-6*^{OR}*; vib-1*$^{-}$	DLL-14(6) x FGSC 2498
Type III escape[2]	unknown	DLL-14(6) x FGSC 18735
WT (FGSC 452)	*ad-8 A*	FGSC
SI (DLL-T2K(0))	*un-24*^{PA}*het-6*^{OR}*; vib-1*$^{-}$ *inl a*	ML Smith
Strain used for RT-qPCR		
FGSC 452	*ad-8 A*	FGSC

[1]Knockout strains screened for type and time of escape are presented in Appendix A.
[2]Escape strains have undetermined mating type, unless specified.
[3]Asteric in *het-6*^{OR*} indicates that *het-6* is mutated and no longer has OR incompatibility specificity.

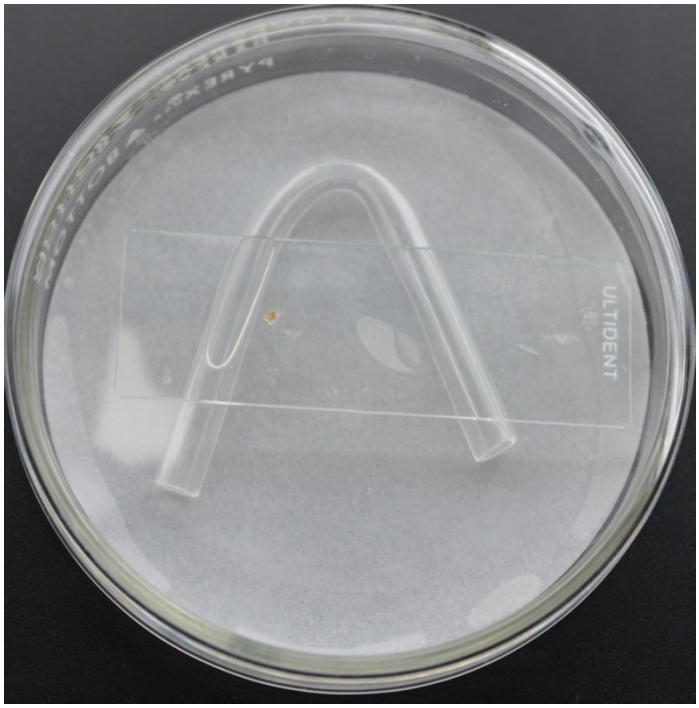

Figure 6. A moist chamber to grow *N. crassa* strains on microscope slide for fluorescent microscopy. Slides are dipped into VMM with required supplements. A 1 mm^3 block of inoculums is then transferred to the medium on the slide. To keep the strains moist, there is a filter paper under the bent glass rod that is moistened often with sterile water. The moist chamber is incubated until the colony has grow into the agar medium, the inoculums block is removed, and the slide is then viewed under a microscope.

Screening for self incompatible progeny bearing the desired knockout:

Knockout strains were crossed to either DLL-14(6) or DLL-T2K(0) depending on their mating type. Crossing plates were incubated for approximately 3 weeks or until they produced perithecia with ascospores. Ascospores where then transferred to a tube containing sterile water. To screen for SI progeny, 50 μL of the ascospore suspension was transferred and distributed on the surface of VMM plates. The spores were placed in a 55°C incubator for 55 minutes to induce germination (Perkins, 1986). After heat treatment, the spores were at room temperature for 12 hours under natural light. Forty of the smallest germlings were then selected under a dissecting microscope (Wild Heerburgg- M4) and transferred into slants containing VMM with supplements. SI colonies were distinguishable after 2 days by characteristic slow growth and aberrant morphology. Single-spore isolates were then spot tested for hygromycin resistance which would indicate that progeny carry the knockout gene. The hygromycin resistant SI colonies were selected for analysis of escape characteristics. From each SI colony five 1 mm^3 blocks were transferred to VMM plates. The plates were incubated at 30°C incubator and monitored every 12 hours for growth rate, escape time and phenotype (Figure 7).

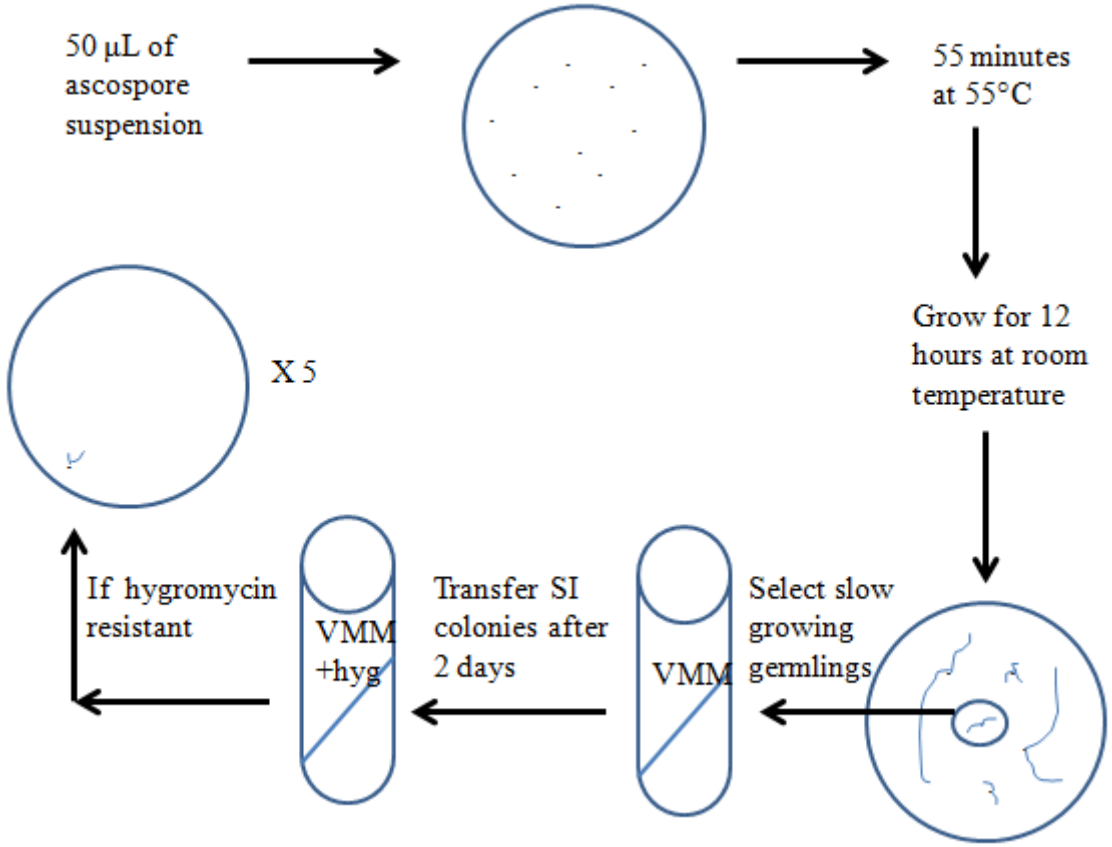

Figure 7. Schematic diagram of screening for self-incompatible progeny that bear the desired gene knockout.

RNA extraction and RT-qPCR:

For RNA extractions and RT-qPCR, FGSC 452 was grown on permeable membrane on top of the medium. After 15 hours of growth the membranes were transferred to media with 0 mM, 80 mM or 120 mM of hydroxyurea (Bioshop, Canada). Cultures were allowed to grow for 0, 1, 2, 5 and 8 hours before harvest and RNA extraction. The mycelium was harvested and flash frozen in liquid nitrogen and crushed using a mortar and pestle. RNA was extracted according to manufacturer's instructions (RNeasy plant mini kit; Qiagen). Extracted RNA was treated with DNaseI (Turbo DNA-free kit; Ambion). cDNA was synthesized with M-MulV reverse transcriptase (New England Bio Labs, Canada). qPCR was performed using KAPA Syber Fast Master Mix (KAPA Biosystems) on a Roto-Gene RG-3000 thermocycler. Primers used for qPCR are presented in Table 3. Agarose gel (1.5%) electrophoresis was used to verify single amplicons with the correct size were obtained. To normalize between qPCR runs, actin (*act-1*; NCU04173) was used as an internal qPCR control. Fold change in expression was calculated for each of the genes using the ΔΔCT method (Livak and Schmittgen, 2001).

Table 3. Primers used for RT-qPCR.

Primer name	Sequence 5' → 3'	Melting temperature (°C)
vib-1 fw	GTATAGGGAGTTTGGTCGAC	52.2
vib-1 rv	GGAAACTCCGACAGAAAGA	51.8
tol fw	GGTTTAGTGGTAGAGGTACTG	51.8
tol rv	CCTCCTCATCCTCGATTT	52.4
het-6 fw	TCTCATGCGTCCTGGTGCTATC	58.8
het-6 rv	CGACTTGGTGGGCTGACGAGT	60.9
pin-c fw	GATTGTGTCGTGGTAGGATG	53
pin-c rv	CGGTCTTGAACAAGGGTTAG	53.2
un-24 fw	GCCTGTTGTCACTCTGTA	53
un-24 rv	AACTTGTTGCTCAGAAAGTGGAG	55.5
act-1 fw	TCTGAATCTCCTGCTCGAAGTCGA	59.3
act-1 rv	ATGGAGTTGAAAGTGGTGACGTGG	59.4

Results

94% of the *un-24*^{PA}*het-6*^{OR} SI colonies escape to wild-type phenotype in a predicted timely manner.

Through homologous recombination, Lafontaine and Smith (2012) developed a self-incompatible (SI) strain that carries the *un-24*^{PA} *het-6*^{OR} haplotype. Colonies of this strain are self-incompatible; they grow very slowly to 39.64 ± 1.55 mm (n=78) in diameter with a characteristic morphology of very thin and tightly packed hyphae for about 4.5 ± 0.39 days at which time a fast growing sector emerges from the colony. This conversion from slow self-incompatible to fast growing form is called "escape" from self-incompatibility (Figure 8). In this study, escape resulted in three different phenotypes. Most often (Type I, 94% of cases) the escape sector exhibited a wild-type (WT) morphology (Table 4) and growth rate. Type I escape colonies produce abundant bright orange-yellow conidia. About 3% of escapes result in a Type II morphology, which is characterized by a growth rate about half that of WT colonies, and a brownish aconidial appearance and raggedy colony margin. The Type II colony typically stops growing as it approaches the edge of the plate (Table 4). However, growth of these arrested colonies resumes upon subculture to fresh medium. The other 3% of escapes result in a 'feathery' morphology (Type III, Table 4). In addition to this characteristic 'feathery' appearance, Type III colonies are yellowish white in color, produce few conidia and grow at an intermediate rate (Escape characteristics are summarized in Table 5). It is worth mentioning that more than one escape colony can emerge from a single SI colony. These escape colonies can be of the same or different types (Figure 9). Since after escape the growth rate increases, it is not

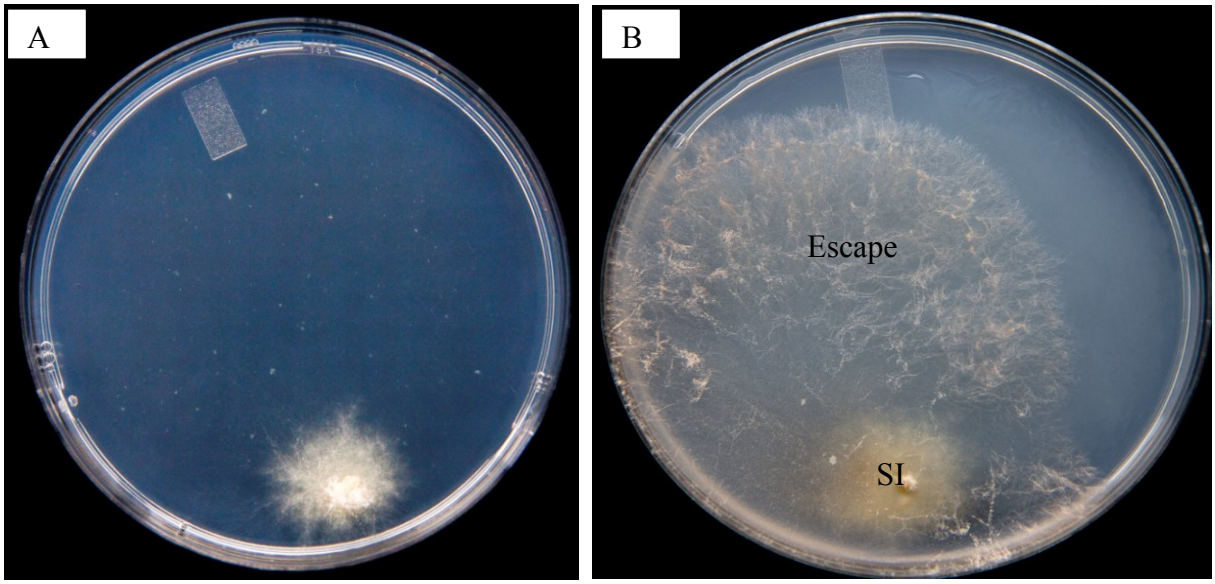

Figure 8. Non-allelic interaction between *un-24*^{PA} and *het-6*^{OR} results in a colony that grows very slowly with flat, densely packed and 'spidery' hyphae which produce few conidia. A) Growth of a self-incompatible *un-24*^{PA} *het-6*^{OR} strain after 4.5 days at 30°C on VMM containing 0.5% inositol. The growth rate of the SI colony is 0.19 ± 0.01 mm/h. B) The escape sector that emerges from the SI colony after 4.5 days has WT growth rate and morphology.

Table 4. Three different *un-24*^{PA} *het-6*^{OR} escape forms have been identified. Individual subcultures (n=93) of self-incompatible strains were allowed to escape. The most frequent type of escape results in Type I escape strains (n=87) that display WT growth rates and morphology. Three colonies of Type II escape were recovered; the Type II form grows slower than WT colonies and has an aberrant morphology. Two colonies of Type III escape were recovered; the Type III form grows slower than WT and shows a distinctive feathery-like morphology. Mean growth rates (+/- SE, at 30°C) are presented ($n > 6$) at top. Pictures were taken of cultures grown at 30°C for 24 and 72 hours after inoculation on VMM with supplement.

	Type I	Type II	Type III
Growth rate (mm/h)	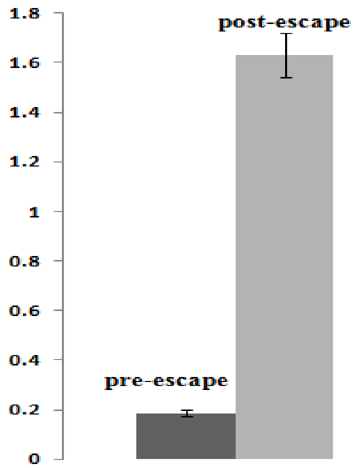	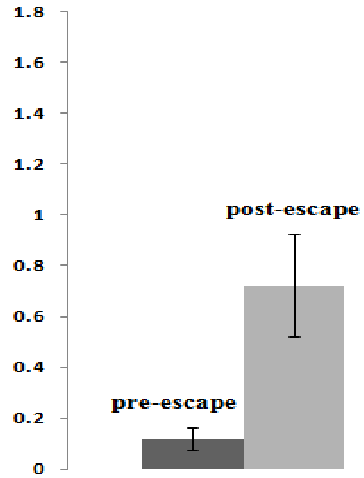	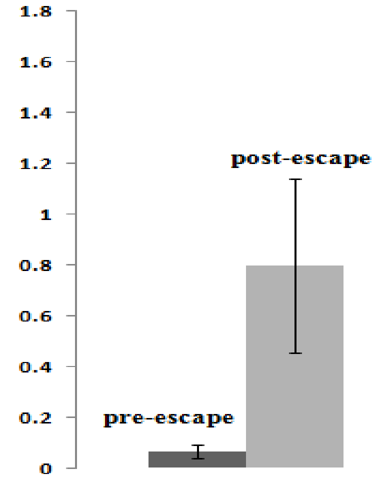
Morphology of post-escapes after 24 hours at 30°C	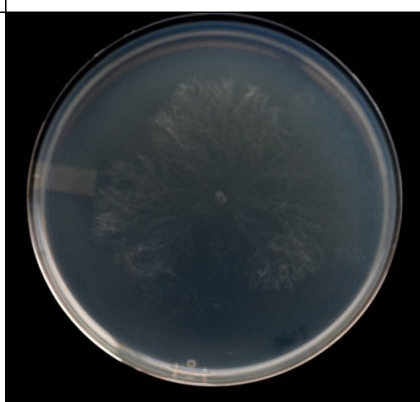	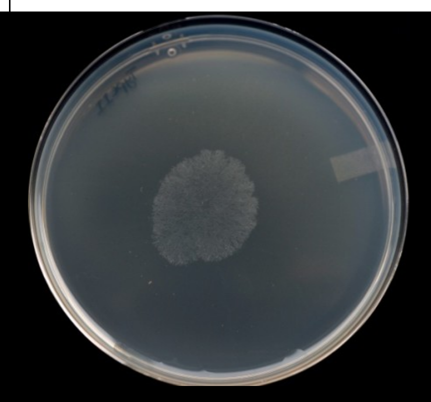	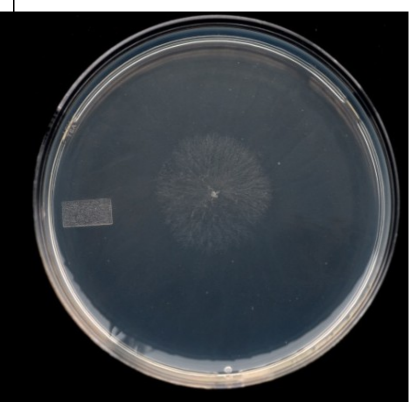
Morphology of post-escapes after 72 hours at 30°C		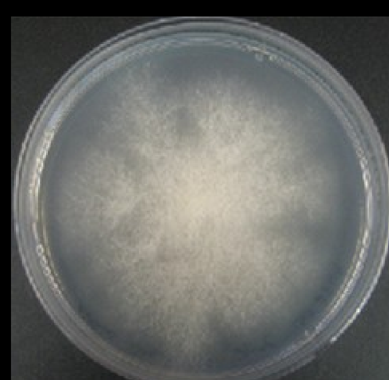	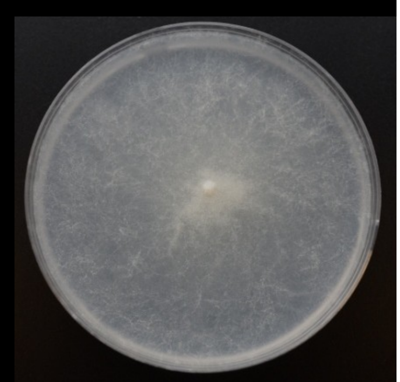
Occurrence (n=93)	94%	3%	3%

Table 5. Behavior and phenotype of three different escape types observed in this study. Hyphal branch angles and diameter were measured in SEM images using Adobe Photoshop.

Escape Type	Post-escape average growth rate (mm/h) (±SE)	Hyphal phenotype	Amount of conidia	Hyphal diameter (μm) (±SE)	Hyphal branch angle (°) (±SE)
Type I	1.6±0.1	Wild-type	Abundant	4.9±0.6	66.3±5.7
Type II	0.7±0.2	Brownish, flat, not touching the edges	Few	3.2±0.3	73±6.1
Type III	0.7±0.3	Yellowish white, flat, feathery	Few	4.72±0.4	77.2±5.6

Figure 9. A Type I and a Type II escape colony emerged from a single SI colony.

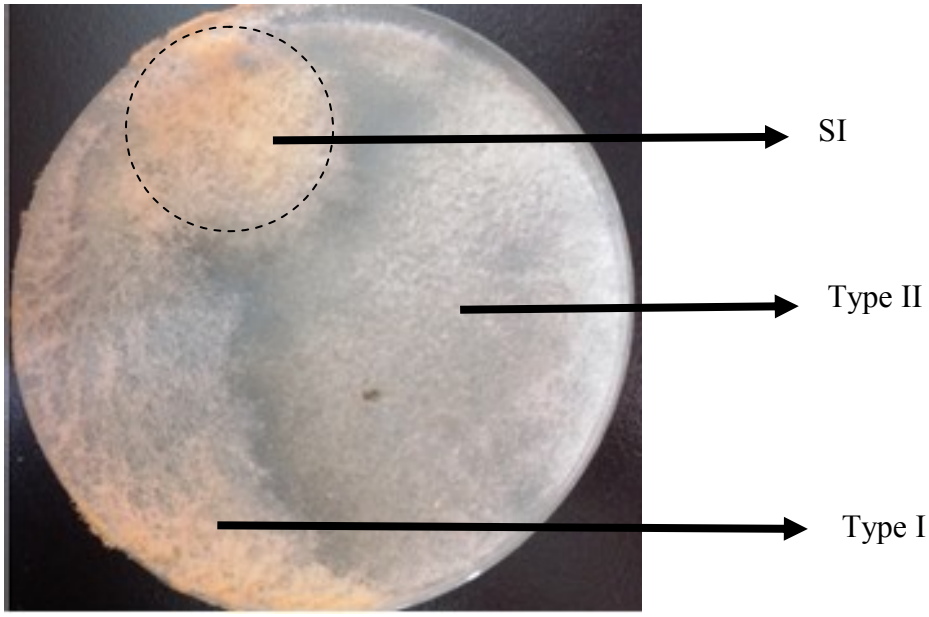

possible to follow all escape colonies and we only investigated the first escape observed from a given SI colony.

Interestingly, the time and SI colony size when escape occurs is quite predictable. At 30°C, escape almost always happens on about day 4.5 after inoculation when the size of the SI colony is about 40 mm in diameter. Prior to 4.5 days, if a small subculture of a pre-escape SI colony is transferred to fresh medium, the resultant colony will grow as an SI and will, itself, escape after about 4.5 days when the diameter of the colony is about 40 mm (Figure 10). In this way, by continuously subculturing SI colonies prior to escape, SI strains can be maintained seemingly indefinitely.

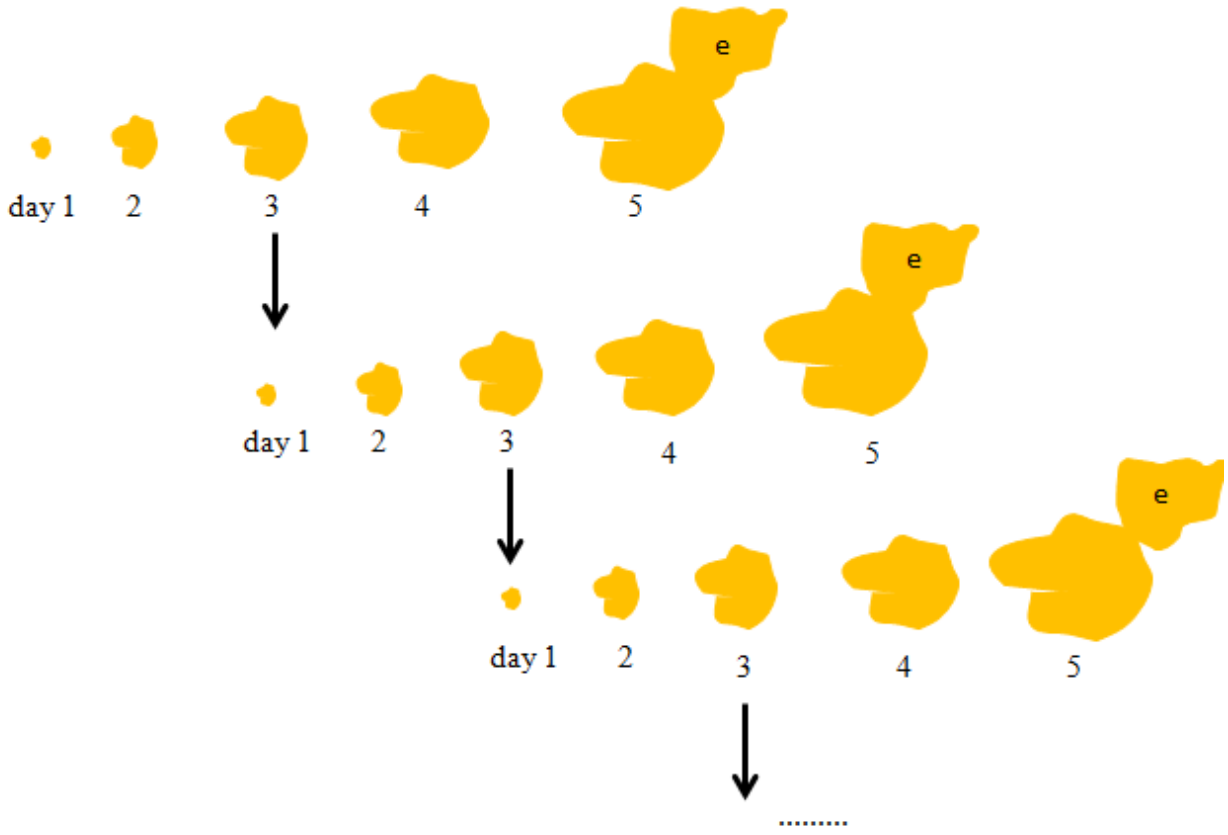

Figure 10. SI colonies grow to about 40 mm for about 4.5 days, at which time an escape sector emerges from the SI colony. When a small inoculum of the SI colony is transferred prior to escape to fresh medium, the resultant colony will grow as an SI colony to about 40 mm in 4.5 days before it escapes. In this manner, it seems that a SI colony can be kept indefinitely. 'e' indicates escape sector.

SEM (Figure 11) revealed that hyphal diameter of WT and Type I post-escape strains are not significantly different ($p=0.7$, 2-tailed t-test, $\alpha=0.05$, $n=8$). Also the hyphal branch angles are similar between Type I and WT strains ($p=0.07$, 2-tailed t-test, $\alpha=0.05$, $n=8$). Comparing Type II escape colonies to WT colonies revealed that hyphal diameter and branch angles are similar in both types ($p=0.08$, 2-tailed, $\alpha=0.05$, $n=8$; $p=0.38$, 2-tailed, $\alpha=0.05$, $n=8$, respectively). Type III and WT colonies are not different in their hyphal diameter a ($p=0.40$, 2-tailed, $\alpha=0.05$, $n=8$) and hyphal branch angles ($p=0.65$, 2-tailed, $\alpha=0.05$, $n=8$). Average hyphal diameter and hyphal branch angles are presented in Table 5.

Thin packed hyphae are the major phenotype of SI colonies that can be observed with microscope and naked eye (Table 6). Type I, II and III escape types are indistinguishable from WT in microscopic images. It is evident from DAPI staining and UV light microscopy that SI hyphae have 3 times fewer nuclei per cell compared to WT, Type I, Type II or Type III post-escape colonies. On average, SI cells contain 6.3 ± 0.5 nuclei, whereas Type I, II and III post-escape cells contain 18.5 ± 0.4 nuclei (Figure 12).

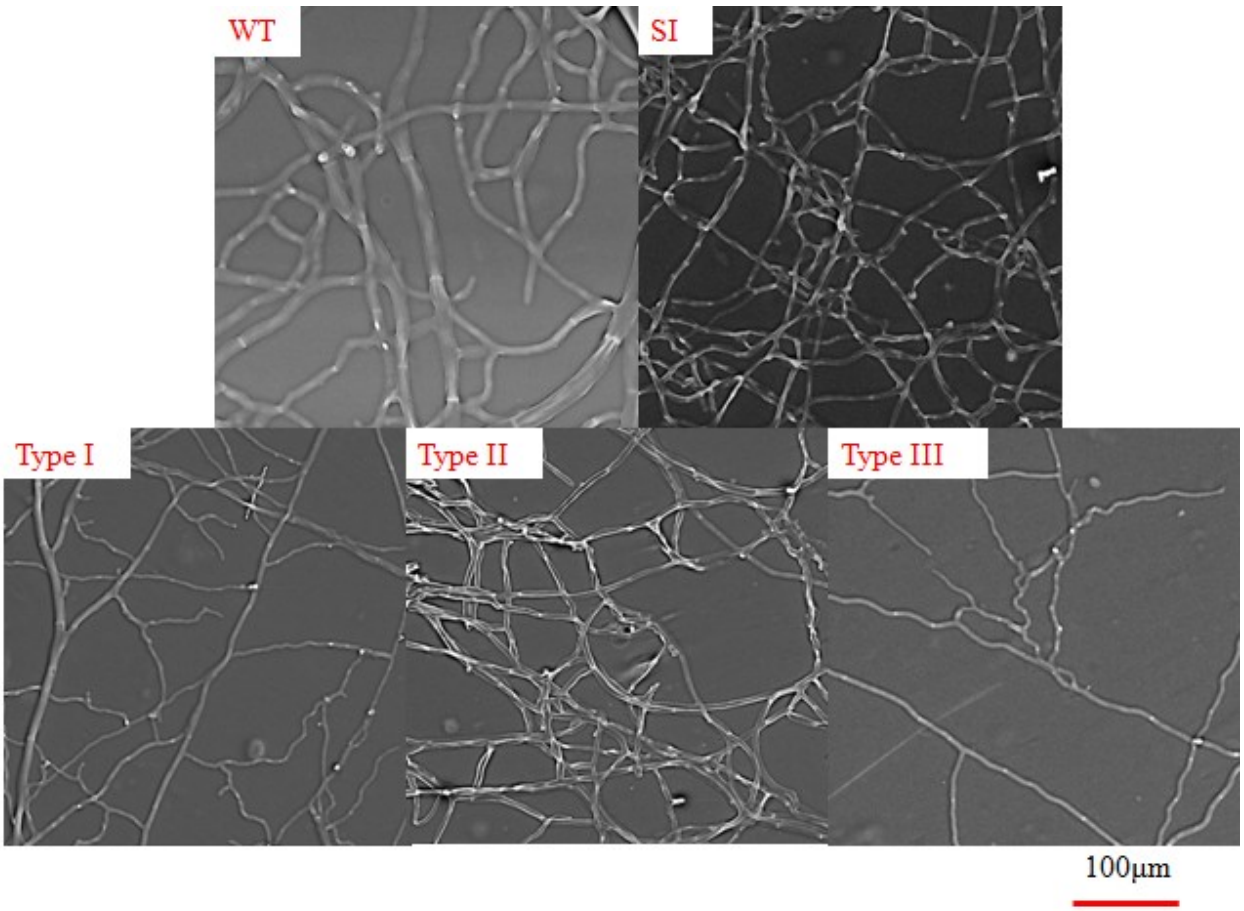

Figure 11. SEM micrographs of WT, SI, Type I, Type II and Type III hyphae.

Table 6. Fluorescent microscopy images of hyphae from WT, SI and 3 types of escape. Colonies were grown on slides dipped into VMM with supplements in a moist chamber. Colonies were then either fixed using 70% ethanol or kept unfixed and then stained with DAPI to visualize and count the nuclei.

	Fixed	Non-fixed
WT	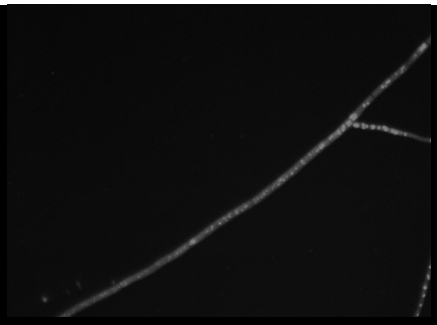	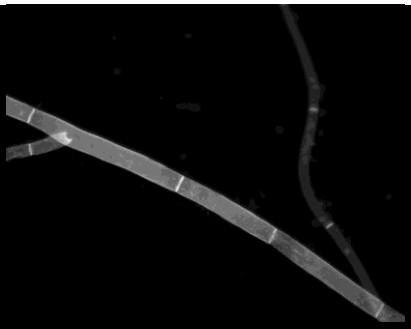
SI	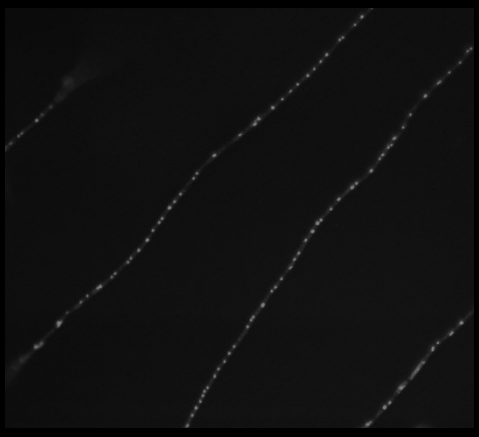	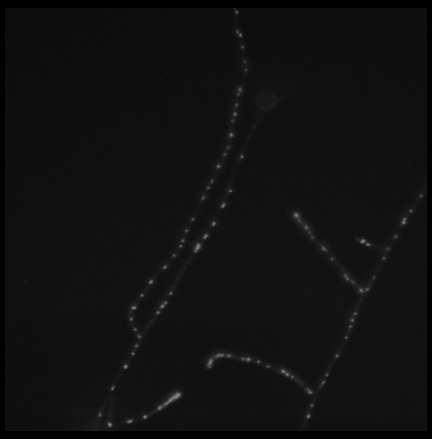

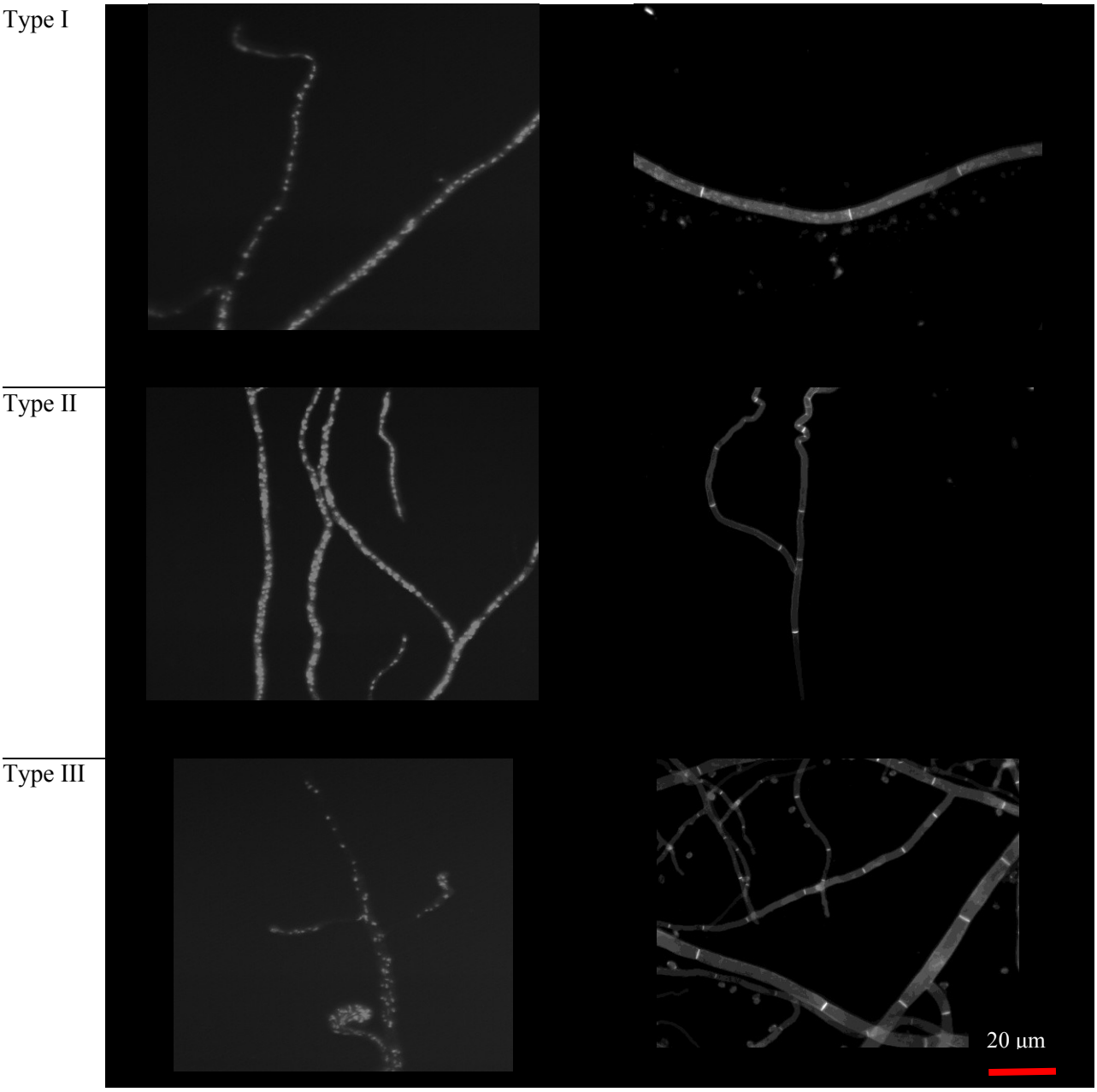
Type I
Type II
Type III
20 µm

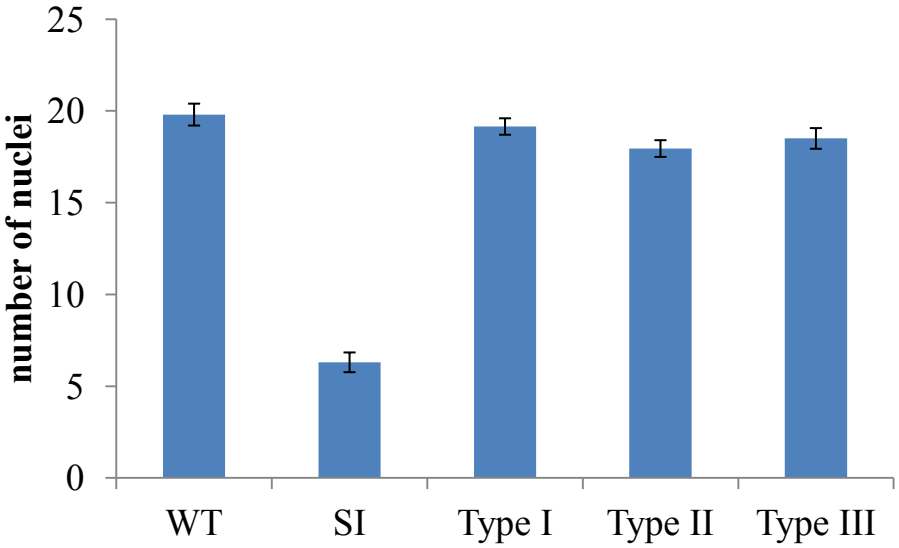

Figure 12. Nuclei were counted in 20 fixed cells from WT, SI, and Type I, II and III post-escape colonies following staining with 0.05% DAPI under fluorescent microscope. As the graph shows, there are on average 3 times fewer nuclei per cell in SI colonies compared to WT or post-escapes. Error bars represent standard error (SE).

Type I escape is due to mutations in the *het-6* locus while Type II escape is associated with mutations in the *vib-1* locus.

As Denis Lafontaine previously mentioned in his M.Sc. thesis (Lafontaine, 2008), heterokaryon compatibility tests showed that Type I escapes are the result of a mutation in the *het-6*^{OR} gene which is denoted as *het-6*^{OR*}. The mutant *het-6*^{OR*} alleles are heritable and co-segregate with *het-6* locus. For sequence analysis of *het-6*^{OR*}, DNA was extracted from *un-24*^{PA} *het-6*^{OR} escapes and the *het-6*^{OR} gene from each was PCR amplified and sequenced. Further sequence analyses by Denis Lafontaine and Iryna Buznytska (unpublished) of 23 independent Type I escape colonies indicated that Type I escape is correlated predominantly with base substitution or, occasionally, small insertion/deletion mutations within the coding region of the *het-6* gene. Both transition and transversion mutations were observed and mutations were not apparently localized to any particular region of *het-6*, including within the HET domain region (Figure 13).

Denis Lafontaine also showed that Type II escape strains are incompatible with both *un-24*^{PA} *het-6*^{PA}, *un-24*^{OR} *het-6*^{OR} and *un-24*^{OR} *Δhet-6*strains. Using PCR/RFLP-based polymorphic markers, he was able to map mutations responsible for Type II escape to the *vib-1* gene (Figure 14).

We have been unable to recover recombinant progeny from crosses involving Type III escape strains and so it has not been possible to map the underlying mutation(s). When crossing Type III escape strains to marker strains *un-24*^{ts} *Δhet-6, un-24*^{PA} *het-6*^{OR}*; vib-1* and *un-24*^{PA} *het-6*^{PA}, it appears that Type III only crosses with *un-24*^{PA} *het-6*^{PA}. Of 40 single ascospores randomly collected and subcultured, only 15 grew, and all of these 15 progeny had a WT phenotype and

the other 25 ascospores were not viable. Also, the original feathery phenotype in the Type III escape strain was observed to change after about 60 hours of growth at 30°C to a whitish color and it produces few conidia. The phenotype is still distinguishable from WT, Type I and Type II escapes, but no longer exhibit hyphae with the feathery appearance.

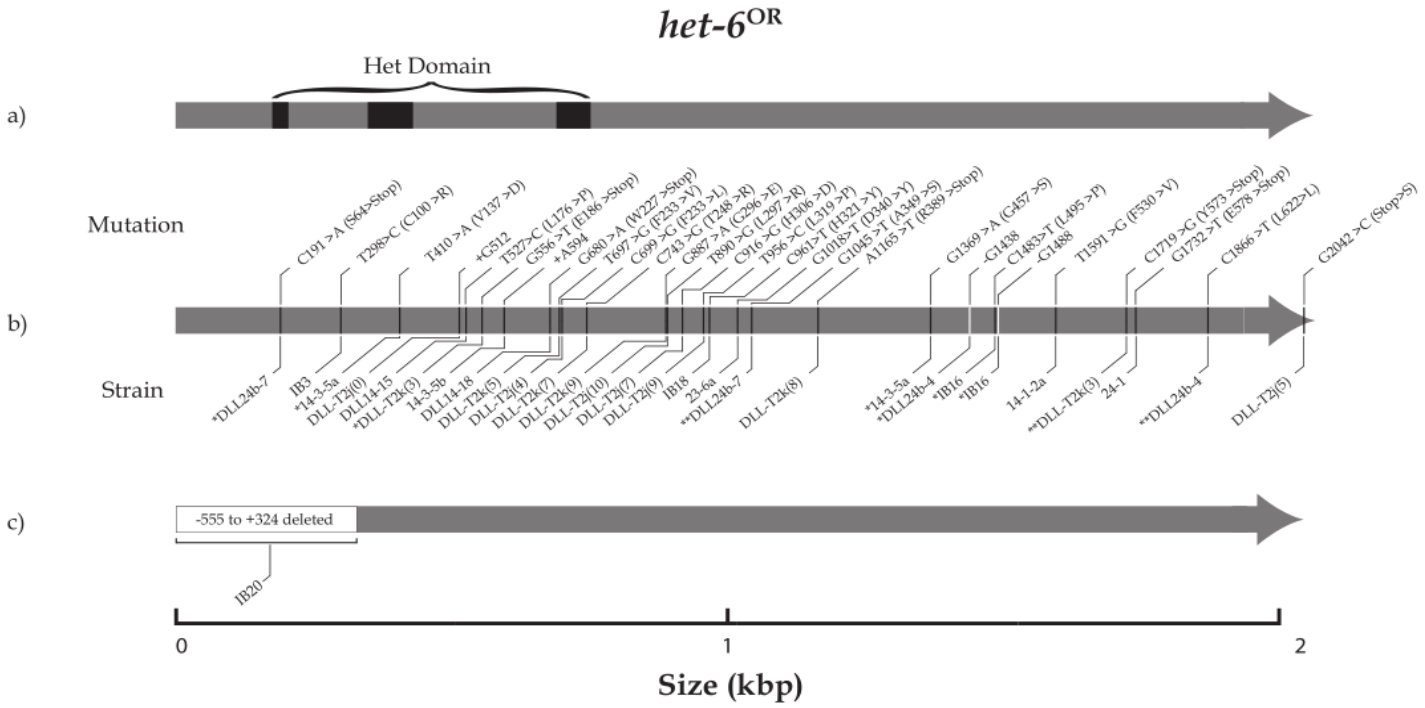

* denotes strains that have more than one mutation in *het-6*
** denotes mutations that are not translated due to the effect of a mutation upstream in the coding sequence

Figure 13. Sequence analysis of the *het-6* gene in 24 independent Type I escape colonies. a) *het-6*^{OR} and three sequence blocks that constitute the HET domain. b) shows the location of mutations in each of the 23 independent escape strains. c) Only one Type I strain was found to have a large deletion that included 555 bp of upstream region and 324 bp of coding region of *het-6*.

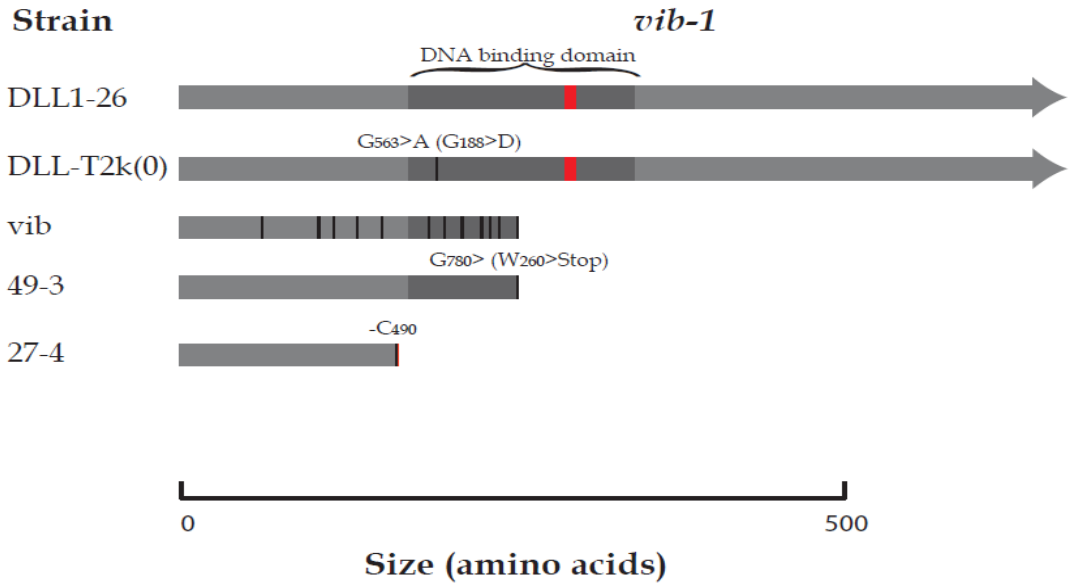

Figure 14. Mutations in the *vib-1* gene that led to three independent Type II escapes. DLL1-26 shows WT *vib-1* with the DNA binding domain highlighted. DLL-T2K(0), 49-3 and 27-4 are from independent Type II escape strains. '*vib*' is a mutant form of *vib-1* that was discovered as a suppressor of *het-c* incompatibility in *N. crassa* (Xiang and Glass, 2004).

Table 7. *het-6* mutations found in 28 Type I escape strains. 4 frame shift mutations are not included in the amino acid changes.

Nucleic acid changes			Amino acid changes				
Transition	Transversion	Frame shift	Synonymous[1]	Non-synonymous	Conserved[2]	Early stop	Stop to amino acid
9	15	4	1	15	1	6	1

[1] Synonymous change occurred together with non-synonymous change at a second position
[2] Chemical and physical properties are conserved between amino acids.

Inferring protein interactions and biochemical pathways involved in escape from *het-6* heterokaryon incompatibility.

Eighty gene knockouts were separately introgressed into SI strains and studied for their effect on SI growth rate, escape timing, colony size when escape occurs and morphology. Any difference from standard escape characteristics would mean a role for that knockout gene in the process (Figure 15). Genes belonging to several functional groups were tested in this way, including genes encoding low fidelity polymerases, and proteins involved in nucleotide excision repair, transcription-coupled repair, double-strand-break repair and base-excision repair. The original idea to account for the predictable timing of escape was that mutations may be directed to *het-6* by an error prone DNA damage repair system. However, all SI strains bearing deletions of a gene involved in the above processes escaped on about day 4.5, similar to control SI strains with no deletions. This indicated that the selected genes were not involved in the escape process.

In considering heterokaryon incompatibility as a type of immune system for filamentous fungi, we investigated effects on escape by deletions of genes with homology to Bcl-6. Bcl-6 acts in germinal B cells to suppress components of the ATR DNA damage response axis so that mutations in Ig loci will result, enabling selection for antibody with maximum affinity for the antigen present in the body. Proteins with a Bcl-6-like zinc finger domain in *N. crassa* (NCU07413, NCU02696, NCU04179, NCU02666 and NCU03975) were tested to find out their effect on escape from HI. All SI strains bearing knockouts at each of these loci escaped similarly to control SI strains. Also, strains with knockouts of homologues of AID (NCU01629, NCU08395) escaped normally. Activation induced deaminase (AID) enzyme, deaminases cytosines to uracils and produces a mismatch U:G lesion. Repair of these lesions in variable locations in Ig loci by error-prone polymerases may result in antibodies with high affinity for the

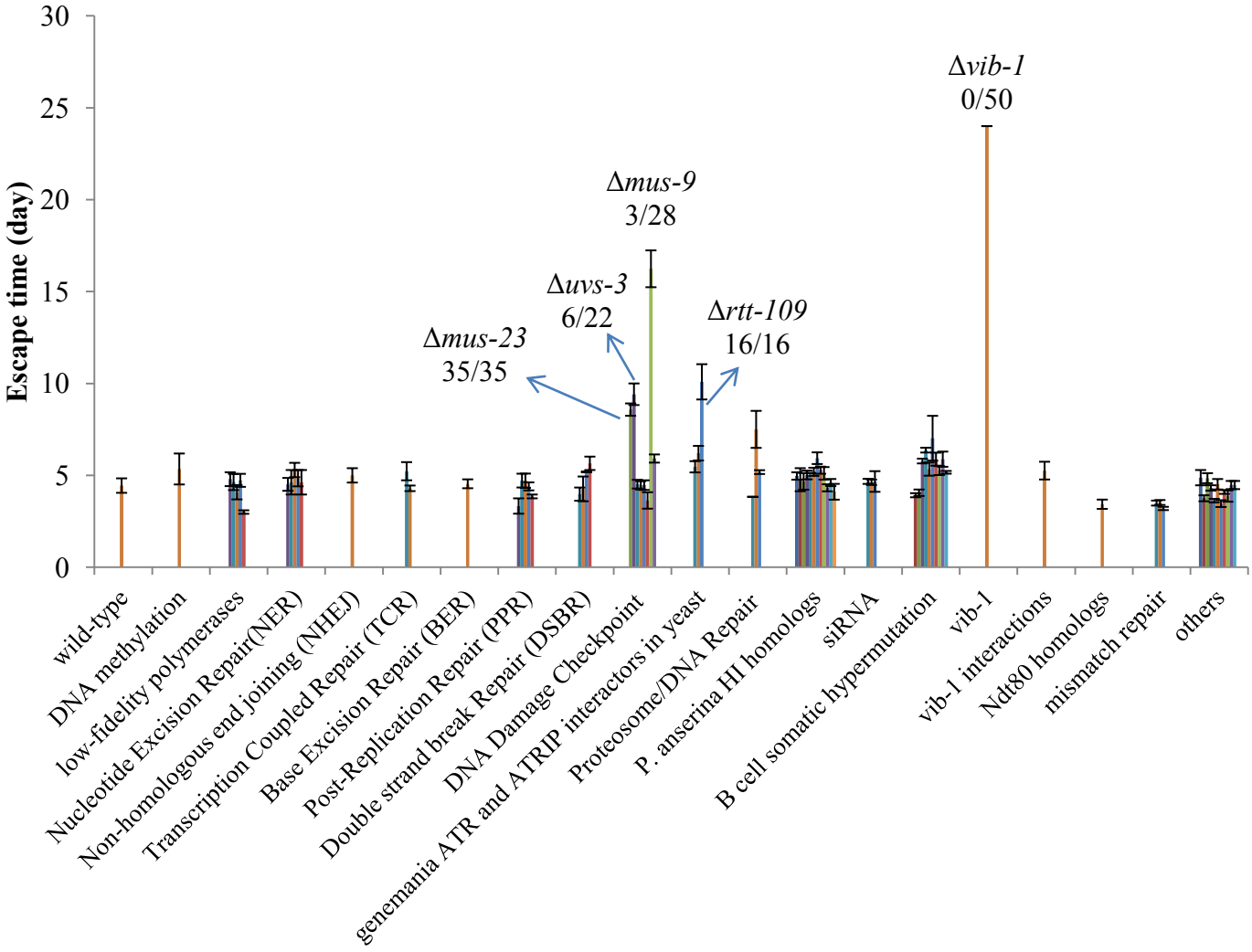

Figure 15. All knockout categories which were screened for their effect on timing of escape (±SE). 80 knockouts (divided into 19 categories shown above) were introgressed into SI background and compared to WT escape timing (shown in left column). Deletions that result in a delay in escape time are designated along with their frequency of escape. Each bar represents average escape time (days ± SE). All gene names in *N. crassa*, and the corresponding orthologues in human and *S. cerevisiae* are given in Appendix A.

antigen (Chandra *et al*., 2015).This result indicates that although the escape process is analogous to B cell hypermutation, it is not apparently homologous.

Next, we targeted genes encoding proteins with known interaction in DNA damage checkpoints in *N. crassa.* When Chk1 (NCU08346, *mus-58*), ATM (NCU00274, *mus-21*) and Chk2 (NCU02814, *mus-59*; NCU02814, *prd-4*) knockouts were each separately introgressed into *un-24*^{PA} *het-6*^{OR} (SI) background, Type I escape occurred at about day 4.5. However, SI strains bearing knockouts in ATR (NCU11188, *mus-9*) and ATRIP (NCU09644, *uvs-3*) showed escape suppression. For example, 4-5 subcultures from each of 6 SI colonies bearing ΔNCU11188:: hph were subcultured (28 colonies in total). Of these, 25 colonies did not escape but continued to grow over a period of weeks as SI colonies until they reached the edge of the plate or the medium dried out. The remaining 3 colonies, escaped on day 8.83 (±0.68SE). Similarly, 4-5 subcultures from 5 SI colonies (22 colonies in total) of ΔNCU09644::hph were evaluated for escape characterization. Sixteen of the subcultures did not escape and the remaining 6 escaped only at 9.24 days (± 1.12SE). Kazama *et al.* (2007) characterized *mus-9* and *uvs-3* genes in *N. crassa* as homologues of ATR and ATRIP genes of human, respectively. ATR and ATRIP are both active in cell cycle checkpoint control. Epistatic and double mutant sensitivity tests further revealed that both *mus-9* and *uvs-3* are involved in the DNA damage checkpoint pathway in *N. crassa* (Wakabayashi *et al*., 2008). Our observations indicated that *mus-9* and *uvs-3* play a role in escape.

Computational interactions for *S. cerevisiae* provided by GeneMania showed interaction and co-expression of LCD1 (ATRIP homologue) and a protein called RTT109. A homologue of RTT109 is also present in *N. crassa* and is denoted as a DNA

damage response protein (NCU09825). SI strains with *rtt109* deleted also exhibited delayed escape (mean escape time=10.09±0.96 SE, n=16). In *N. crassa,* RTT109 is a histone acetyltransferase which acts on lysine 56 of H3 (Zhang *et al*., 2013). RTT109 and H3K56 mutants in *N. crassa* are defective in homologous recombination, which implicates a role for RTT109 in the DNA damage pathway. Of note, acetylated H3K56 is more abundant in *N. crassa* treated with hydroxyurea (Zhang *et al.,* 2013). Hydroxyurea is considered to specifically inhibit ribonucleotide reductase function (Krakoff *et al*., 1968). This is intriguing in the context of *het-6* incompatibility given that we hypothesize that HET-6^{OR} protein interacts with UN-24^{PA}, the Panama form of the large subunit of RNR in *N. crassa* to elicit an incompatibility response.

N. crassa strains with mutations in *mus-23* are also known to be mutagen sensitive. The gene *mus-23* encodes the homologous protein to yeast Mre11p. In *S. cerevisiae* Mre11p and two other proteins, Xrs2 and Rad50p, make up the MRX complex which is important for recruitment of Tel1p to the site of DNA damage. The double mutants *mus-23/rtt109* and *mus-23/uvs-3* are both nonviable in *N. crassa* (Watanabe *et al.,* 1997). When tested in our assay, 35 out of 35 of the SI strains knocked out for *mus-23* (NCU08730) escaped, however they escaped on day 8.58 (±0.34SE) which is later than observed in WT background. It can be inferred that among genes tested for their effect on escape, only those involved in checkpoint control and sensing stalled replication forks are seemingly implicated in escape.

It should be noted that while SI strains deleted for *mus-9*, *uvs-3*, *rtt109* and *mus-23* exhibit suppression of escape (reduced incidence and/or delay in escape), each showed

some escape activity. Only the *vib-1* gene knockout was never observed to escape to a Type I form. As mentioned earlier, *vib-1* mutations are responsible for Type II escapes. In Type II escape, self-incompatibility is only partially suppressed; the Type II growth rate is about half of that of the WT and Type II colonies produce few conidia. Interestingly, when looking closer at the VIB-1 amino acid sequence, we found a p53-like transcription factor domain (SSF4917) which is also found in human NFkappaB and Ndt80 in *S. cerevisiae* (Figure 16). This gave rise to the question, does VIB-1 function in part in *N. crassa* like p53 function in mammalian cells?

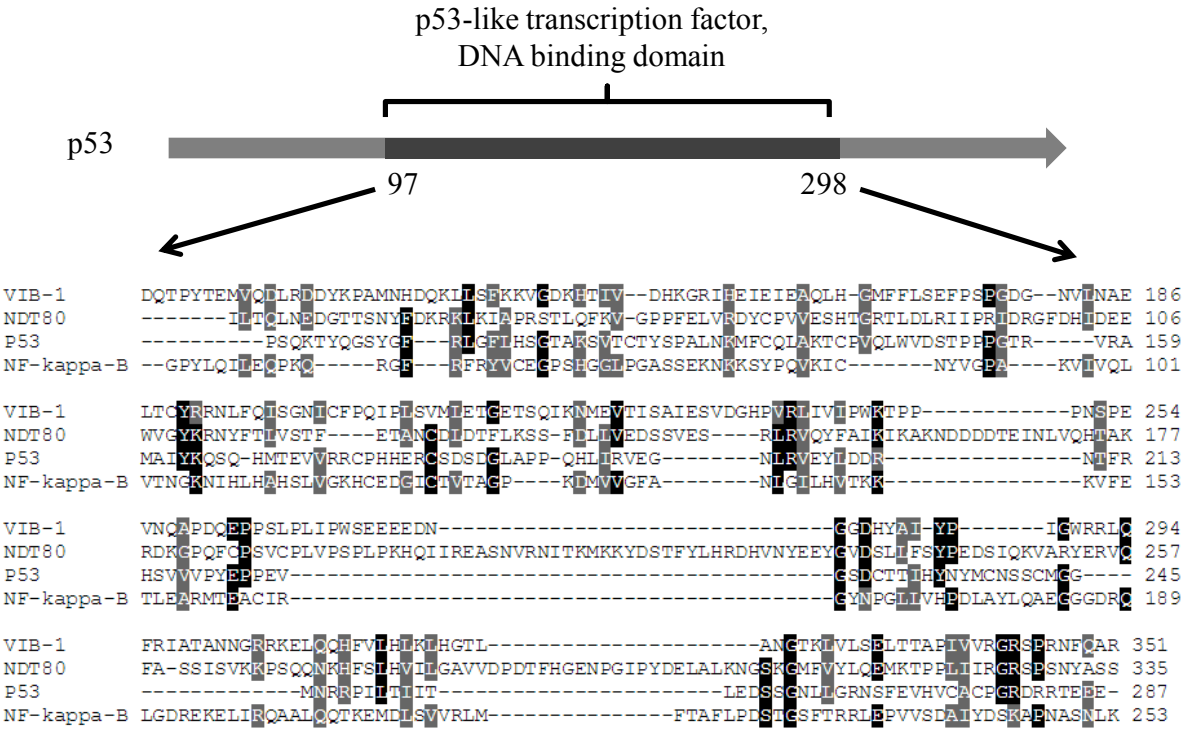

Figure 16. Transcription factor DNA binding is shown on p53 (between amino acids 97 to 298) along with sequence similarities in VIB-1, Ndt80p and NF-kappa-B. The sequences of the 4 proteins were aligned using MUSCLE. Black background shows identical amino acids among all sequences. Gray background shows amino acids with similar R-groups. White background shows dissimilar amino acids. Sequence Manipulation Suit (SMS) is used to shadow conserved amino acids. Conserved amino acids are highlighted based on 3 or more of the sequences.

Effect of exogenous DNA damage agent hydroxyurea on expression levels of *vib-1*, *het-6*, *tol*, *pin-c* and *un-24*

If VIB-1 acts as a signaling hub, similar to p53, we would expect DNA damage, due to nucleotide deficiencies, would activate *het-6*. To investigate the effect of an exogenous DNA damaging agent, *N. crassa* WT strain (FGSC00452) was grown on permeable membranes until a colony diameter of 12.26 mm ± 0.33 SE was reached. The membrane and colony was then transferred to media containing either 0, 80 or 120 mM of HU and grown for 0, 1, 2, 5 and 8 hours on HU before harvest, RNA extraction and RT-qPCR (Figure 17). RT-qPCR analysis of the extracted RNA from each of the colonies is presented in (Figure 18). The housekeeping gene used to normalize CT values between datasets is actin (*act-1*). Figure 19 shows that CT value for actin in control and experimental conditions are approximately the same meaning that experimental conditions had minimal effect on actin expression (average 1/CT =0.07±0.0006SE). RNA extraction of the samples that were exposed to 120 mM HU for 1 hour had DNA contamination. Therefore the 120 mM HU treatments for 1 hour were excluded from further analysis.

Figure 18 shows that after 1 hour exposure to 80 mM HU, expression levels of *vib-1* go up by 3.5 fold relative to no-HU control. Also, the expression of the genes that were previously reported (Dementhon *et al*., 2006) to be controlled by VIB-1 go up, except for *pin-c*. Of note, expression of *het-6* increases by about 7 fold. These increases in transcript abundance that are evident at 1 hour HU exposure are transient and generally

not evident at later time points with the exception of *un-24*, the expression of which increases to 47.8 folds compared to that of the control at 8 hours HU exposure.

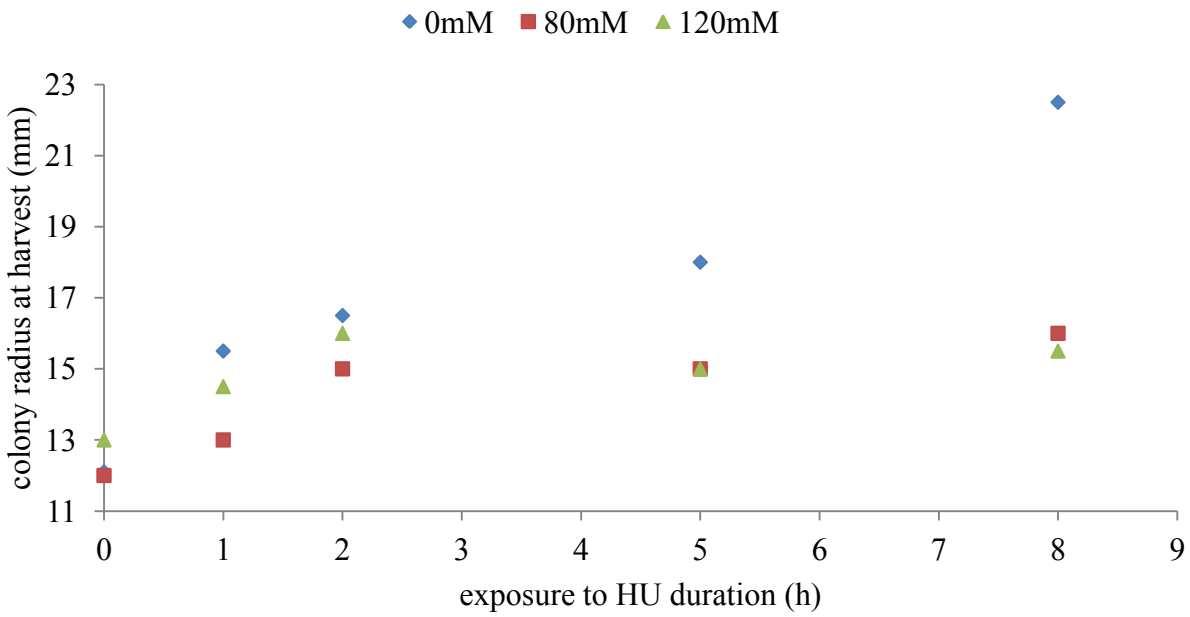

Figure 17. Colony size at time of harvest for RNA extraction.

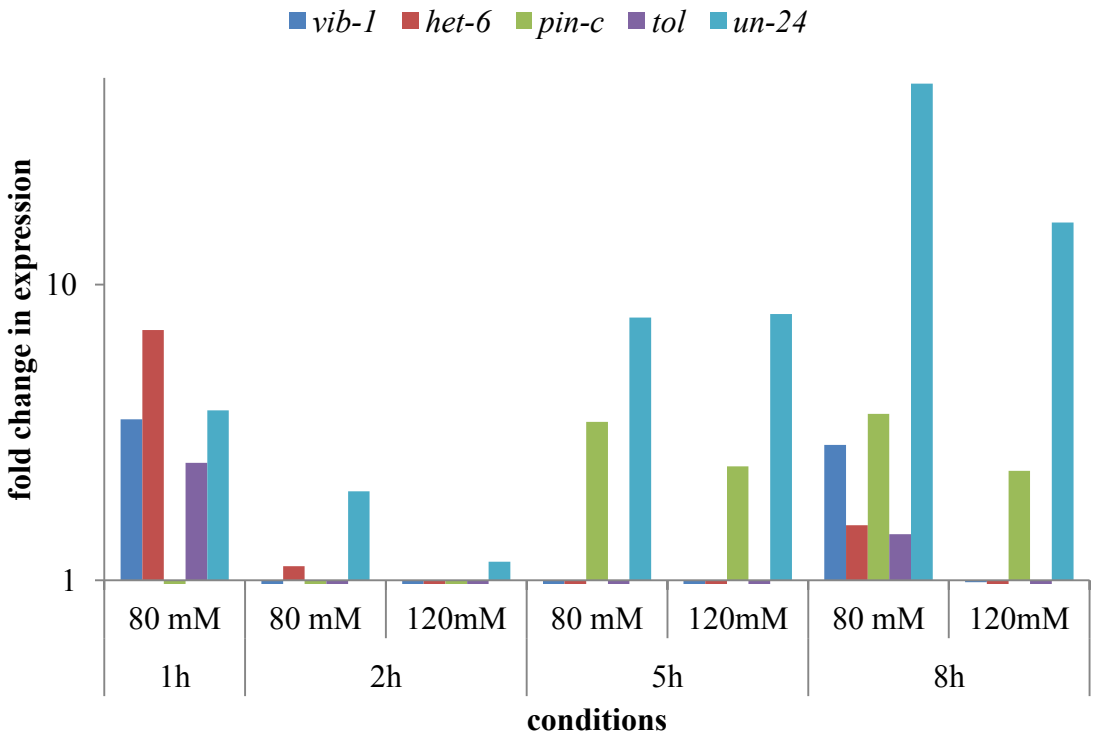

Figure 18. Fold change in expression of *vib-1*, *het-6*, *pin-c*, *tol* and *un-24*. *act-1* expression was used as an internal control to normalize between data sets. Exposure to 0 mM of HU for 0, 1, 2, 5 and 8 hours were used as control for 80 mM and 120 mM HU exposure for the same period of time. ΔΔCT method is used to calculate fold change expression of each of the genes. Y axis is on logarithmic scale. Fold change is compared to same time of growth on 0mM HU.

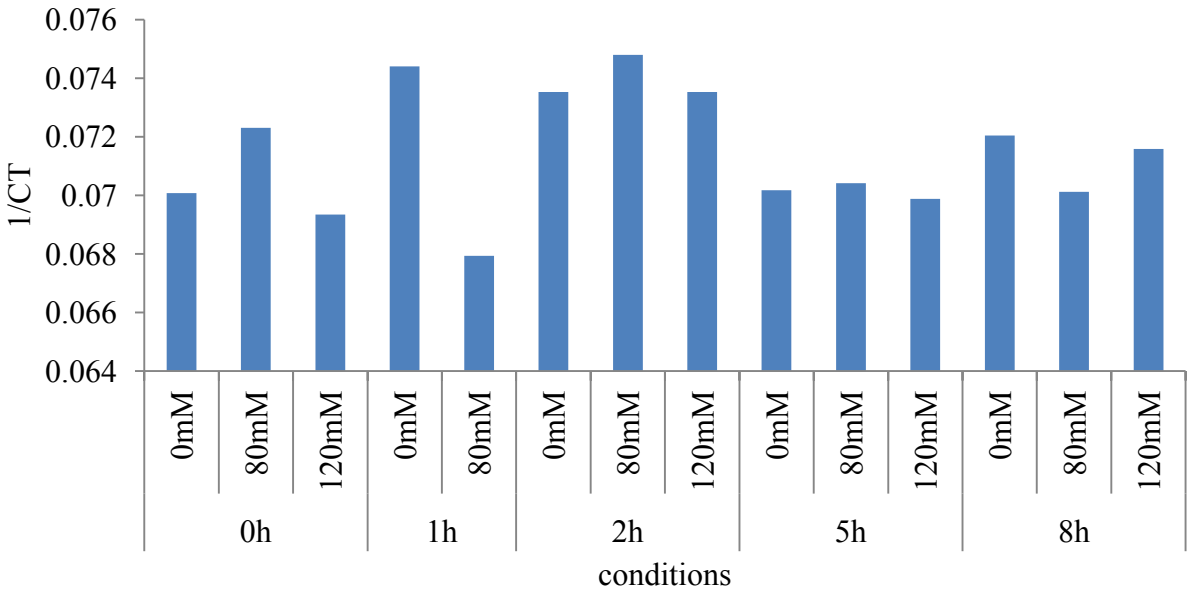

Figure19. 1/CT for the housekeeping gene actin (*act-1*) in all control and experimental conditions. Actin is used as a control to normalize between treatments. The average 1/CT for actin (*act-1*) is 0.07 ± 0.0006SE.

Discussion

The *het-6* locus comprises two genes, *het-6* and *un-24*. Previous research indicates that specific allele combinations, *un-24*^{OR} *het-6*^{PA} and *un-24*^{PA} *het-6*^{OR}, are primary causes of incompatibility associated with this locus. In this study we examined incompatibility due to *un-24*^{PA} *het-6*^{OR} interactions. Here, HET-6^{OR} is hypothesized to bind to UN-24^{PA} and disrupt essential protein RNR that is required for DNA replication. It is not known how the two genes are now genetically linked together but it can be hypothesized that *het-6* was recruited to a position that is next to *un-24* and this gave rise to the incompatibility complex. By depleting dNTP pools, the incompatible reaction between *un-24*^{PA} and *het-6*^{OR} would likely promote growth arrest or initiation of PCD which may signal to an escape pathway, as a means by which the cell can overcome the incompatibility.

To gain insight into biochemical pathway involved in escape, we used the strain *un-24*^{PA} *het-6*^{OR} (Lafontaine and Smith, 2012) in which this incompatible combination of alleles occurs in the same nucleus. To sustain the strain in the lab and avoid escape, a mutation in *vib-1* was introduced to this strain (DLL-T2K(0) in Figure 14). Mutations in *vib-1* partially suppress incompatibility between *het-6* and *un-24*. Our *un-24*^{PA} *het-6*^{OR}; *vib-1* strain is stable, but grows slower than wild-type colonies and produces few conidia. This observation indicates that *vib-1* may play a role in promoting the incompatibility process in *N. crassa*. Additional support comes from work done by Dementhon *et al.* (2006) on the effect of *vib-1* on incompatibility and programmed cell death resulting from HI. They found that *vib-1* also controls incompatibility between *het-c* and *pin-c*.

They also found that death following HI is a result of differential localization of *vib-1* to hyphal compartment. Putting all these observations together, it can be inferred that HI is controlled by *vib-1* and since *vib-1* strains never escape, it may be that initiation of programmed cell death in the colony triggers escape.

It has never been directly studied whether *het-6* heterokaryon incompatibility is accompanied by programmed cell death. However, the microscopy work done in this study (Table 6) indicates that many cells in our SI colonies are dead. We looked at SI cells stained with DAPI to visualize nuclei. We repeated the microscopy using both fixed and non-fixed hyphae. In the fixed state, the nuclei were observable in cells of all wild-type, SI and escape colonies. In the non-fixed state, very few nuclei were stained in wild-type and escape colonies. However, nuclei in SI colonies were readily evident in both fixed and non-fixed hyphae. Given that DAPI is pumped out of, or excluded from live *N. crassa* cells, this observation suggests that may be many cells in SI colonies are either dead or they are dying.

That escape occurs at a predictable time is remarkable. We saw that escape happens at around day 4.5. But another aspect of colony escape to consider is colony size. Almost all escapes in this study happened when the colony achieved a diameter of about 40 mm. We hypothesize that the escape signal is size dependent rather than time dependent. To test this hypothesis we tried to keep the colony in its pre-escape state by subculturing a small piece of a 3 day-old colony to new medium. The colony would then resume growth in the new medium and would escape when its size reached 40 mm in diameter (Figure 10). This behavior suggests that escape is determined by size, and not

time, and suggests that "quorum sensing" plays a role in the escape process. "Quorum sensing" is a signaling system first recognized in bacteria. By exchanging chemicals, bacteria sense conspecific cell density. Bacteria modulate their gene expression based on cell density appropriate to their environment. For example, they may change their virulence, form biofilms, modulate bioluminescence reactions, etc. (Miller and Bassler, 2001; Reuter *et al.,* 2016). To date "quorum sensing" is best characterized in bacterial species and little is known about the process in eukaryotes. The escape signal may be a manifestation of quorum sensing. More work has to be done to further investigate this idea. For example, preliminary work in our laboratory indicates that macerated pre-escape inoculums spread over 15 mm area gives rise to escape in less than 4.5 days. However, more study needs to be done to test the hypothesis that escape is initiated through quorum sensing.

Three types of escape are distinguished in this study. Type I escapes are mostly the result of a point mutation or occasional small insertion/deletion within the coding region of *het-6* (Figure 13). This indicates that the *het-6* gene is extremely sensitive to mutational perturbations along the entire length of the gene. It is still not clear why 94% of the time the mutations happen in *het-6* but the observations suggest that there is some specificity to, or targeted at *het-6*. In several cases, two sectors were observed to arise from the same SI colony. We subcultured distinct Type I sectors from 5 SIs and, in each case, found different mutations in *het-6*. This indicates that independent mutations may occur at the time of escape. It can also be hypothesized that some other mutations are happening in the pre-escape colony but they do not lead to escape. Type II escapes are

due to mutation in *vib-1* (Figure 14) and happens about 3% of the time. Type II escapes does not result in suppression of incompatibility since the colony grows at half wild-type rate and produce few conidia. Type III escape colonies initially show a distinct feathery morphology and they produce a few conidia. This morphology appears to be transient, converting to a whitish, aconidiated colony. However, Type III escapes are distinguishable from Type I and Type II, notably in being partially barren when crossed with marker strains. Unlike Type I and Type II, Type III phenotype could not be transmitted through sexual crosses. Because of this, we were unable to map the mutation.

The *het-6* gene in each of 29 Type I escape strains was sequenced. Mutations that are responsible for Type I escape are mostly base-substitution mutations, as opposed to insertions and deletions. It is interesting that among the Type I mutations, transversions are more common than transitions (15 to 9, respectively) since, normally, transition mutations far exceed transversions (Collin *et al*., 1994). This bias may provide information of the underlying mechanisms of escape and should be further explored. The point mutations lead almost exclusively to non-synonymous amino acid changes or early translation stops. The only synonymous change was observed in one Type I escape strain that had two mutations; the synonymous mutation was downstream of a G insertion (frame shift). Two single nucleotide insertions and 2 single nucleotide deletions were also observed. Only one escape strain resulted from a large deletion in contrast to an earlier study that examined escapes of *het-6* self-incompatible partial diploids (Smith *et al*., 1996). It seems that in all escapes examined in the present study, mutations that result in non-synonymous amino acid changes are favored. It can be proposed that the change in

the protein product of *het-6* gene is important for change in the incompatibility behavior of the *het-6* gene product. In 3 Type II escape strains sequenced, we saw two transitions and one frame shift. The transitions gave rise to one early "stop" codon and one non-synonymous, non-conserved amino acid change. All the changes affected the DNA binding domain. Since, only 3 Type II strains have been sequenced, it is not possible to make comparisons between the mutation spectra of *het-6 vs vib-1*. Additional sequence analyses of *vib-1* mutants are needed for meaningful comparisons.

In this study, we investigated the effect of 80 gene knockouts on escape occurrence, timing and phenotype (Figure 15). We introgressed each gene separately into the SI background and monitored growth rate and escape time. For each gene knockout, we selected at least 2 SI progeny which were then subcultured to establish at least 5 colonies. This way we could control if the knockouts produce any genetic predisposition for a certain type of escape.

All gene knockouts tested tended to favor the Type I escape. This indicates that none of these genes altered the apparent specificity towards mutations in *het-6*. We also observed that from a single SI colony two different types of SI would arise (Figure 9). Therefore, it can be concluded that the knockout genes did not exert any genetic predisposition and that any escape is independent of the other one even when they arise from the same SI colony.

Apart from *Δvib-1* which never escapes, our study of 79 other gene knockouts showed us that 4 gene knockouts are interfering with escape. They either never escape or they escape later than normal. We investigated the growth rate of the wild-type strains

bearing these knockouts. The result shows that these knockouts have no appreciable effect on growth rate in an otherwise wild-type background. Therefore, the interaction between incompatible genes and these knockouts is significant. Orthologues of all 4 of these genes are involved in DNA damage checkpoint in human (Figure 15, Table 1, and Appendix A). *mus-9*, *uvs-3*, *mus-23* and *rtt109* are all implicated in DNA repair in *N. crassa* as well. However, their interactions are not completely understood and likely differ from those of human and yeast orthologues.

MUS-9 and UVS-3 are checkpoint proteins in *N. crassa* (Kazama *et al.,* 2007) but their signaling pathway is not known. MUS-23 is another checkpoint protein in *N. crassa* and has significant homology with human MRE11 and *S. cerevisiae* Mre11p. Other than knowing that *N. crassa mus-23* mutants are defective in recombinational repair (Watanabe *et al.,* 1997), nothing is known about its mode of action. RTT109 mutants are also defective in recombinational repair. It is an acetyltransferase for H3K56 that is more abundant in tissue treated with hydroxyurea (Zhang *et al.,* 2013). Although, our understanding of DNA damage checkpoints and repair signals are very limited in *N. crassa*, we can hypothesize that the process that leads to escape is interconnected to DNA damage checkpoints. This is very interesting because *het-6* incompatibility involves interactions between UN-24 and the HET-domain protein, HET6. One of the triggers of stalled replication fork is depleted dNTP pools. The repair signal is then initiated in the system to recruit DNA damage proteins to the site of damage and activate repair systems. The presence of *vib-1* as a control switch for incompatibility is also intriguing in this system. VIB-1 has some characteristics that make it similar to mammalian p53 which is a

hub in the DNA repair system. Like p53, VIB-1 is a transcription factor, it is important for programmed cell death and in its sequence it has a p53-like DNA binding domain. Also, *vib-1* is a homologue of yeast Ndt80. When, accumulation of ssDNA arrests cell cycle during pachytene, Mec-1 dependent checkpoint is activated to initiate DNA repair. If at this point Ndt80 becomes phosphorylated and activated, the cell will exit pachytene arrest. Therefore, Mec-1 inactivates Ndt80 transiently until the repair signal is off (Gray *et al.,* 2013). This may be similar to the role *vib-1* plays in escape. VIB-1 may be important to enable arrested incompatible colonies to undergo repair and ultimately escape. It can be hypothesized that VIB-1 is regulated by activation of MUS-9 dependent checkpoint and when repair is finished, MUS-9 activates VIB-1 to exit cell cycle arrest.

Based on this knowledge, we proposed a model for escape from *het-6* incompatibility (Figure 20).

The model is explained as follows. In a wild-type strain any modulations in the *het-6* gene affect the normal function of RNR and as a result there is a perturbation in dNTP pools present in the cell. One of the signals that can activate the DNA damage response in a cell is imbalances in dNTP pools. The signal is sensed by RTT109 and MUS-23 and then recruitment of MUS-9/UVS-3 to the site of damage occurs. At this point the decision is by VIB-1 to either arrest the growth and promote programmed cell death or repair the damage. Repair happens via a mutation in either *het-6* to totally abolish incompatibility or to *vib-1* itself to only partially restore growth.

It seems that the *N. crassa* interactions are unlike those in *S. cerevisiae* or mammalian systems. In both of those cases, Mre11 accompanied by Rad50 and

Nbs1/Xrs2 are important to clamp ATM/ Tel1 to the site of DSB. In our study, *Δmus-21* and *Δnbs-1* had no effect on escape, but *Δmre-23* strains escaped late. It can be inferred that Mre-11 orthologue in *N. crassa* is a sensor for MUS-9/UVS-3 DNA damage checkpoint rather than MUS-21. Also, it can be suggested that in *N. crassa* MUS-23 has some redundancy. If it was the only sensor, then its absence would totally abolish escape under our model. One of these other sensors could be RTT109. It has been shown that *rtt109* transcript levels go up in HU treated cells (Zhang *et al*., 2013). In our model MUS-9/UVS-3 act as the transducers. The interaction between protein products of ATR and ATRIP seems to be conserved between mammalian, *S. cerevisiae* and *N. crassa*. Also, our results show that not all of the strains with *Δmus-9* and *Δuvs-3* are defective in escape. It can be inferred that as in *S. cerevisiae*, *mus-21* is able to phosphorylate some of *mus-9* effectors and send the signal for escape. Maybe, *mus-21* is not vital for the cell unlike ATM in mammalian cells (Figure 21).

We checked all known effectors of DNA damage checkpoint in *N. crassa* for their effect on escape. Orthologues of Chk1 and Chk2 had no effect on escape. *vib-1* has never been characterized to be involved in DNA damage response. However, at least in the context of HI it has the characteristics of an effector. Its presence is important for the fate of an incompatible colony either for PCD or for suppressing incompatibility.

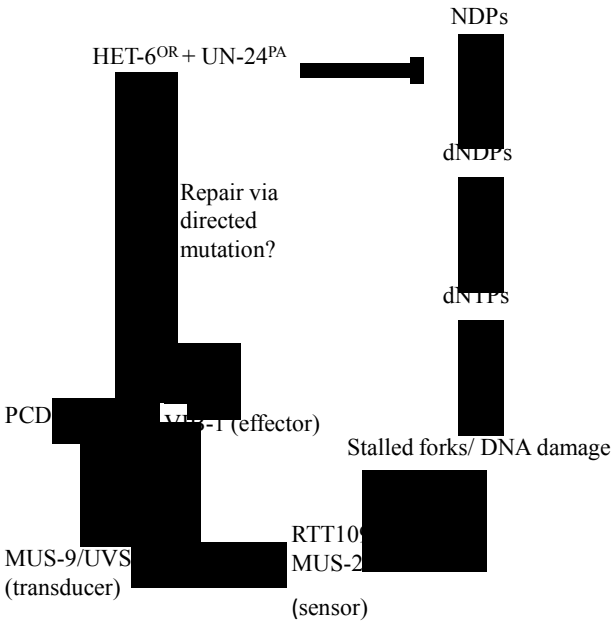

Figure 20. Proposed model of escape through directed mutation in *het-6* gene. The incompatibility reaction between *het-6*^{OR} and *un-24*^{PA} modulates the healthy function of RNR. This may result in imbalances in dNTP pools that are sensed by DNA damage checkpoints as damage or a stalled fork. The signal is transduced in the cell through a series of phosphorylations starting from RTT109 and MUS-23 and recruitment of MUS-9/UVS-3 to the site of damage. Through VIB-1 the fate of the cell is decided which can range from PCD to repair via directed mutation. It should be noted that VIB-1 is a transcription factor and has a binding domain upstream *het-6*^{OR}, *vib-1* and other incompatibility-associated genes in *N. crassa*.

Figure 21 puts our understanding of DNA damage checkpoint activation during escape into the general schematic of ATR dependent checkpoint activation in mammalian cell.

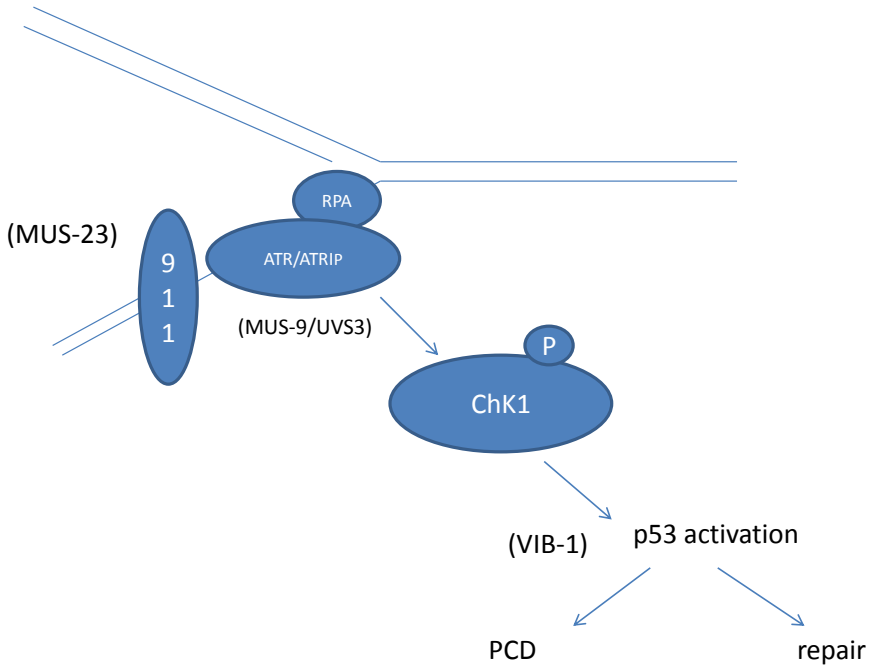

Figure 21. Repair of ssDNA through ATR dependent checkpoint pathway. Protein names in parenthesis show where the mutants involved in escape may fit.

Our search for error-prone polymerases and other DNA repair systems did not result in a single mutant making escape pathway deficient, with the exception of mutations in *vib-1*. However, it should be noted that these pathways are redundant. Whenever one is mutated, others deliver the function and this may make it difficult to find one single repair system responsible for mutagenesis in escape. However, some evidence shows that recombinational repair is involved in this process. One piece of evidence is that ATR-dependent checkpoint usually activates homologous recombination to repair ssDNA. Since MUS-9 is an orthologue of ATR, it can be hypothesized that recombinational repair is also involved in escape. Other evidence is that in *N. crassa Δrtt-109* and *Δmus-23* show decrease in levels of HR and recombinational repair respectively. All together, it seems that HI results in stalled replication forks and accumulated ssDNA and recombinational repair is the repair system involved in escape.

It is very interesting to note that early studies reported that mutations resulting in 'mutagen-sensitivity' also effect escape in partial diploids with duplicated heterozygote *mat* loci. In these studies, mutants of *uvs-3* and *mus-9* increased the partial diploid instability and the self-incompatible strains escape faster. In these strains escape is the result of either deletion of one copy or changes in one mating locus to make it compatible with the other locus (Shroeder, 1986; Newmeyer *et al.,* 1978; Schroeder, 1970).

The most important assumption in this model is that DNA damage activates VIB-1and as a result HET-6 or any other HET-domain protein. To test this assumption we used hydroxyurea (HU), which is known to inhibit RNR functions and lead to DNA damage and then we measured levels of *het-6*, *pin-c*, *tol*, *vib-1* and *un-24*. Use of HU as a

genotoxic agent is very interesting in this system. It is known that HU interrupts RNR and as a result dNTP pools are depleted in the cell which in turn interferes with cell cycle and replication. In this sense, we can mimic the *het-6*-associated HI system where incompatibility between *het-6* and *un-24* interrupts dNTP pools and replication.

RT-qPCR analysis (Figure 18) show that 1 hour of exposure to 80 mM HU increases *het-6* transcript levels by 7 folds and *vib-1* transcript levels by 3.5 fold. It is plausible for *vib-1* as the regulator to show less change. Increase in transcript levels of *het-6* as a result of DNA damage fits into our model. It is also interesting to see that *un-24* levels are seemingly increasing constantly over the eight hour experiment. It seems that when HU is interfering with RNR function, the cell tries to compensate by making more RNR. Exposure to 120 mM HU had lesser effect on transcript levels. It may be that the dosage was very toxic to the colony. Unfortunately our qPCR study has only one biological replication. In future studies, one can look at transcript around the first hour of exposure. This may give a better understanding of modulations in expression levels. Also, it seems that 120 mM HU exposure is very toxic to the cells and DNA damage, repair and growth is more visible in colonies exposed to 80mM.

In this study, we investigated interactions that are involved in escape from *het-6* incompatibility. Interestingly, our result suggests a connection between DNA damage checkpoint and escape. Therefore, this system not only is used to shed light on incompatibility in filamentous fungi and in turn other organisms, it also can be used to increase our knowledge of DNA damage signaling and DNA repair. Involvement of RNRL in this specific incompatibility locus can give us a tool to study RNR interactions

with DNA repair as well as incompatibility. For example, RNR activity can be monitored in an incompatible system to what is the evolutionary advantage of the genetic linkage between *un-24* and *het-6* genes. Also the effects of exogenous genotoxic stress (e.g. HU) on RNR and *un-24* can be compared to incompatible strains. This may also lead to an understanding of functions other than heterokaryon incompatibility for *het-6* and its protein product.

The pivotal point of this study is escape, its exact timing and the direction of mutations to within *het-6* and the heterokaryon incompatibility suppressor, *vib-1*. These results are in line with other studies done to investigate HI and escape. The unifying theme is that escape always is a result of mutation, either large deletions or point mutations, in loci that are involved in PCD. In *N. crassa*, investigated incompatibility interactions in *het-c*, *het-6* and *het-e* are all modulated by *vib-1*, meaning that escape is either halted in mutant *vib-1* strains or escape is a result of mutation directed to *vib-1*. Therefore, a more inclusive model may explain escape from heterokaryon incompatibility.

All of these observations are pointing toward one result and that is escape is due to directed mutations. Therefore, studying escape and the interactions involved in the process can help understand the diversifying selection governing non-self recognition systems.

Appendices

Appendix A. All gene knockouts used in this study.

Classification	Strain[1]	genotype	Gene I.D.	*N. crassa* annotation	*Saccharomyces cerevisiae* annotation (BLASTP E value)	*Homo sapiens* annotation (BLASTP E value)
wild-type	C9-2 :: un24 PA	un-24 PA het-6OR	N/A	N/A	N/A	N/A
DNA methylation	22118	dim-2	NCU02247	DNA methyltransferase dim-2	N/A	DNA (cytosine-5)-methyltransferase 1 (2e-28)
low-fidelity polymerases	12058	rev7	NCU06577	MUS-26; REV7	Rev7 (0.0087)	Structure Of Polymerase-interacting Domain Of Human REV1 (7e-9)
	12929	rev1	NCU02053	MUS-42; REV1	Rev1 (7.8e-81)	DNA repair protein REV1 (2e-97)
	12608	poli	NCU06757	DNA polymerase Tau	Rad30 (5.2e-05)	DNA polymerase iota (7e-28)
	13372	polh	NCU01936	DNA polymerase Eta	Rad30 (2.9e-37)	DNA polymerase eta isoform 3 (e8e-50)
	12042	polk	NCU02457	DNA-directed polymerase kappa	Rev1 (1.9e-09)	polymerase kappa isoform 4 (3e-50)
Nucleotide Excision Repair (NER)	13431	rad23	NCU07542	rad23-like protein	Rad23 (1.1e-23)	RAD23 (2e-72)
	20199	rad4	NCU06585	Rad4 family protein	Rad4 (1.2e-25)	UV excision repair protein RAD23 homologue B (2e-72)
	14432	rad1	NCU07440	MUS-38	Rad1 (1.4e-131)	DNA repair protein complementing XP-C cells (3e-29)
	12062	rad2	NCU07498	DNA excision repair protein Rad2	Rad2 (5.1e-121)	DNA repair endonuclease XPF (4e-80)
	12527	rad7	NCU03649	hypothetical protein	Rad7 (2.6e-17)	DNA repair protein complementing XP-G cells (3e-64)
Non-homologous end	20277	mus-51	NCU08290	ATP dependent DNA helicase I	Ku70 (2e-29)	N/A

joining (NHEJ)						
Transcription Coupled Repair (TCR)	13121	rad-26	NCU07837	DNA repair protein Rhp26/Rad26	Rad26 (4.8e-206)	DNA excision repair protein ERCC-6 (0)
	13916	rad-28	NCU06679	histone acetyltransferase type B subunit 2	Hat2 (1.3e-53)	histone-binding protein RBBP4 isoform b (4e-139)
Base Excision Repair (BER)	12357	mus-18	NCU08850	mutagen sensitive-18; UV-endonuclease UVE-1	N/A	N/A
Post-Replication Repair (PPR)	11444	rad-18	NCU05210	ultraviolet sensitive-2; postreplication repair E3 ubiquitin-protein ligase rad-18	Rad18 (6.5e-31)	E3 ubiquitin-protein ligase RAD18 (6e-30)
	12067	rad-5	NCU09516	DNA repair protein rad-5	Rad5 (4.4e-144)	helicase-like transcription factor (1e-83)
	16323	rad-5	NCU02913	DNA repair protein rad5	Rad5 (2.2e-52)	helicase-like transcription factor (6e-62)
	11337	rad-5b	NCU07975	DNA repair and recombination protein RAD5B	Rad5 (1.1e-51)	helicase-like transcription factor (8e-99)
	11756	rad-5c	NCU05246	DNA repair and recombination protein RAD5C	Rad5 (4.7e-55)	helicase-like transcription factor (4e-81)
Double strand break Repair (DSB)	12433	mei-3	NCU02741	MEI3	Rad51 (7.3e-124)	DNA repair protein RAD51 homologue 1 isoform 1 (3e-176)
	18989	hypothetical protein	NCU08806	hypothetical protein	Rad55 (2.6e-06)	DNA repair protein RAD51 homologue 2 isoform 3 (1e-9)
	15578	hypothetical protein	NCU10077	hypothetical protein	N/A	N/A
	13434	mus-53	NCU06264	DNA repair and recombination protein MUS53	Dnl4 (2.6e-94)	DNA ligase 4 (3e-113)
DNA Damage Checkpoint	12933	mus-23	NCU08730	mutagen sensitive-23	Mre11 (8.3e-123)	double-strand break repair protein MRE11A (1e-134)
	11168	uvs-3	NCU09644	ultraviolet sensitive-3	N/A	N/A
	11162	mus-21	NCU00274	mutagen sensitive-21	Tel1 (9.7e-96)	serine-protein kinase ATM (7e-138)

	11169	prd-4	NCU02814	serine/threonine-protein kinase chk2	Dun1 (3.0e-65)	serine/threonine-protein kinase CHK2 (2e-83)
	12018	mus-59	NCU02751	mutagen sensitive-59;serine/threonine-protein kinase	Rad53 (1.4e-45)	serine/threonine-protein kinase CHK2 (2e-83)
	11164	mus-58	NCU08346	serine/threonine protein kinase, variant,serine/threonine protein kinase	Chk1 (3.7e-74)	CHK1 checkpoint homologue (7e-49)
	DLL-T4a	mus-9	NCU11188	mutagen sensitive-9; phosphatidyl inositol 3-kinase; ATR	Mec1 (2.5e-126)	serine/threonine-protein kinase ATR (1e-166)
	12674	rca-a	NCU06049	DNA damage response protein RcaA	N/A	nibrin (2e-12)
Genemania ATR and ATRIP interactions in yeast	12048	pin-4	NCU05343	R3H domain-containing protein	Pin4 (2e-41)	solution structure of the second RNA binding domain of RNA binding motif protein 23(8e-04)
	19229	csm-3	NCU01858	chromosome segregation in meiosis protein 3	Csm3 (5e-13)	TIMELESS-interacting protein isoform 1 (3e-11)
	12340	rtt-109	NCU09825	DNA damage response protein Rtt109	Rtt109 (5e-14)	N/A
Proteosome/DNA Repair	12675	ddi-1	NCU05292	DNA damage-inducible protein 1	Ddi1 (2.9e-57)	protein DDI1 homologue 2 (7e-71)
	12414	mus-8	NCU09731	mutagen sensitive-8	Rad6 (7.4e-67)	ubiquitin-conjugating enzyme E2 B (6E-79)
	16329	dph-1	NCU03028	deubiquitination-protection protein dph1	Dsk2 (2.0e-52)	ubiquilin 4 (1e-06)
P. anserina HI homologues	16857	NACHT	NCU00874	hypothetical protein	N/A	N/A
	11945	NACHT	NCU08565	hypothetical protein	N/A	N/A
	12532	NACHT	NCU08705	hypothetical protein	N/A	N/A

	13941	NACHT	NCU02897	hypothetical protein	N/A	N/A
	12862	NACHT	NCU05316	pfs domain-containing protein	Hos4 (2e-09)	ankyrin-1 (8e-49)
	12118	NACHT	NCU07168	hypothetical protein	N/A	N/A
	12338	NACHT	NCU09760	hypothetical protein	N/A	N/A
	11987	NACHT	NCU08537	hypothetical protein	N/A	N/A
	11270	idi-4	NCU08055	b-ZIP transcription factor IDI4	N/A	N/A
	11925	modin	NCU07121	modin	N/A	N/A
	12377	gna-2	NCU06729	guanine nucleotide-binding protein alpha-2	Gpa1 (3.2e-74)	guanine nucleotide-binding protein G(o) subunit alpha (1e-103)
	11868	serin endopeptidase	NCU00263	serin endopeptidase	Kex2 (0.39)	PCSK2 protein (9e-5)
siRNA	15891	dcl-1	NCU08270	dicer-like protein 1;Sms-3	Irc3(0.005)	DICER1 (5e-61)
	11155	dcl-2	NCU06766	dicer-like protein 2	Mph1(2e-05)	DICER1 (1e-24)
	qde-2::unPA	qde-2	NCU04730	post-transcriptional silencing	N/A	chain A, human argonaute2 A481t mutant bound to T1-a target RNA (2e-72)
B cell somatic hypermutation	19554	hypothetical protein	NCU01629	Cytosine deaminase	Swi5(1e-13)	SP1 protein (2e-14)
	20272	dim-1	NCU08395	pre-mRNA splicing factor Dim1	Dib1 (2e-65)	thioredoxin-like protein (4e-80)
	3975	zinc finger protein 58	NCU03975	zinc finger protein 58	Bcl-6 (2e-20)	zinc-finger protein 3(1e-33)
	11101	Cytosine deaminase	NCU07413	Cytosine deaminase	Bcl-6 (1e-6)	chain A, crystal structure of the Vif-binding Domain of human Apobec3f(0.39)
	11347	zinc finger protein	NCU02699	zinc finger protein	Bcl-6 (3e-20)	zinc-finger protein 383(3e-26)
	11132	sah-1	NCU04179	C2H2 transcription factor	Bcl-6 (1e-19)	zinc-finger protein 143 (1e-25)
	11344	NSDC	NCU02666	NSDC	Bcl-6 (4e16)	SP3(6e-17)
	16008	hypothetical	NCU06907	hypothetical protein	Swi5(3e-24)	zinc finger and BTB domain-containing

		protein				protein 7C (6e-15)
	15425	adenosine deaminase	NCU00438	adenosine deaminase	N/A	adenosine deaminase-like protein isoform 1 (3e-43)
	11483	C2H2 transcription factor	NCU00038	C2H2 transcription factor	Pzf1(3e-19)	transcription factor IIIA (2e-31)
vib-1		vib-1	NCU03725	vegetative incompatibility block-1	Ndt80 (0.018)	unnamed protein product (0.33)
vib-1 interactions	17936	ime-2	NCU01498	protein-kinase-8	Ime2 (7E-80)	MAK protein (4e-78)
Ndt80 homologues	12180	Ndt-80 like DNA binding family	NCU04729	Ndt-80 like DNA binding family	N/A	N/A
	12534	fsd-1	NCU09915	female sexual development-1	Ndt80 (3e-13)	N/A
mismatch repair	12529	msh-2	NCU02230	DNA mismatch repair protein msh-2	Msh2 (0)	MSH2 (0)
	12524	msh-3	NCU08115	DNA mismatch repair protein Msh3	Msh3 (9e-131)	MSH3 (0)
	11970	mlh-1	NCU08309	DNA mismatch repair protein mutL	Mlh1 (0)	MLH1 (0)
Other	15721	tfb5b	NCU06646	RNA polymerase II transcription factor B subunit 5	Tfb5 (4.1e-11)	general transcription factor IIH subunit 5 (4e-05)
	11189	rad-9	NCU00470	DNA repair protein Rad9	N/A	cell cycle checkpoint control protein RAD9A isoform 1 (2e-24)
	12053	DNA repair protein	NCU05966	DNA repair protein	Pso2 (7.9e-06)	DNA cross-link repair 1A (7e-16)
	18735	hypothetical protein	NCU02608	Elongation factor methyltransferase	Efm2 (5e-24)	protein-lysine methyltransferase METTL21D isoform b (3e-08)
	18151	hypothetical protein	NCU07957	hypothetical protein	Esc2 (0.1)	N/A
	11914	histone-lysine N-	NCU06266	histone-lysine N-methyltransferase	Dot1(9e-64)	chain A, structure of the catalytic domain of human Dot1l, a non-set domain

		methyltransferase				nucleosomal histone methyltransferase (1e-26)
	19786	pik1a	NCU10397	phosphatidylinositol 4-kinase PIK1a	Pik1 (9e-124)	phosphatidylinositol 4-kinase beta isoform 3 (4e-78)
	11191	rad-1	NCU16423	hypothetical protein	N/A	N/A
	11548	pzl-1	NCU07489	phosphatase-Z-like-1	Ppz1(0)	serine/threonine-protein phosphatase PP1-alpha catalytic subunit isoform 1 (5e-146)
	15739	hypothetical protein	NCU01366	hypothetical protein	Ulp2(2e-10)	sentrin-specific protease 6 isoform X3 (1e-14)
	12530	col-24	NCU05383	fungal specific transcription factor	Mlh3 (1e-28)	N/A

[1] All numbers are the FGSC numbers.

Appendix B. Crosses, their time of escape and diameter at escape.

Crosses	average escape time (day)	+/-SD	+/- SE	Escape count	average max growth rate (mm/h)	diameter at escape(mm)
C9-2::unPA	4.44	2.04	0.39	27	n/a	40.00
dim-2::unPA	5.35	4.04	0.84	23	n/a	40.00
T2K(0) X 12058 (Δrev7::hph)	4.79	0.84	0.38	5	0.30	47.16
DLL14-1 X 12929 (Δrev1::hph)	4.64	0.98	0.44	5	0.30	51.79
T2K(0) X 12608 (Δpoli::hph)	4.08	n/a	0.39	1	0.28	45.10
DLL14-1 X 13372 (Δpoln::hph)	4.73	0.87	0.35	6	0.30	54.11
T2K(0) X 12042(Δpolk::hph)	3.01	0.19	0.10	4	0.33	35.75
T2K(0) X 13431(ΔRad23::hph)	4.51	0.86	0.35	6	0.19	32.35
DLL14-1 X 20199(ΔRad4::hph)	4.63	0.94	0.67	2	0.20	37.78
T2k(0) X 14432(ΔRad1::hph)	5.29	n/a	0.39	2	0.12	43.57
DLL14-1 X 12062(ΔRad2::hph)	4.84	0.7698	0.44	3	0.24	38.94
DLL14-1 X 12527(ΔRad7::hph)	4.63	0.94	0.67	2	0.23	35.92
Ku70	5.00	n/a	0.39	n/a	0.09	40
T2k(0) X 13916(ΔRad28::hph)	5.23	1.31	0.49	7	0.21	40.31

DLL14-1 X 13121(ΔRad26::hph)	4.30	0.51	0.15	11	0.20	31.72
DLL14-1 X 12357(Δmus-18::hph)	4.54	0.59	0.24	6	0.21	36.31
T2k(0) X 11444(ΔRad18::hph)	3.33	0.59	0.42	2	0.17	35.65
T2k(0) X 12067(ΔRad5::hph)	4.72	1.06	0.38	8	0.20	36.23
DLL14-1 X 16323(ΔRad5::hph)	4.71	n/a	0.39	1	0.20	45.64
T2k(0) X 11337(ΔRad5b::hph)	4.40	0.58	0.22	7	0.19	29.13
DLL14-1 X 11756(ΔRad5c::hph)	3.85	0.18	0.10	3	0.22	29.48
DLL14-1 X 12433(ΔRad51::hph)	3.98	0.95	0.36	7	0.17	30.25
DLL14-1 X 18989(ΔRad55::hph)	4.26	1.17	0.67	3	0.26	33.65
T2k(0) X 15578(ΔCTiP::hph)	5.19	0.00	0.00	7	0.340	62.97
T2k(0) X 13434(Δmus-53::hph)	5.66	0.89	0.36	6	0.21	43.90
DLL14-1 X 12933(ΔRad32::hph)	8.58	1.98	0.34	35	0.047	19.01
DLL-14-1 X 11168(Δuvs-3::hph)	9.41	2.75	0.59	6 out of 22	0.19	54.74
T2K(0) x 11162 (ΔATM :: hph)	4.52	0.71	0.24	9	0.19	31.04
DLL14-1 X 11169 (Δprd4::hph)	4.46	0.60	0.23	7	0.17	27.63
DLL14-1 X 12018 (Δmus-59::hph)	4.47	0.74	0.26	8	0.17	27.94
DLL14-1 X 11164 (Δmus-58::hph)	3.64	1.10	0.45	6	0.23	28.75
DLL14-1 X DLL-T4a (ATR::hph)	16.23	5.30	1.00	3 out of 28	0.19	55.44
DLL14(6) x 12674 (Δrca 1::hph)	5.92	0.59	0.22	7	0.16	32.77
T2K(0) X 12048(ΔPIN4::hph)	5.47	0.97	0.30	10	0.11	20.00
DLL14(6) X 19229(ΔCSM3::hph)	6.21	2.28	0.39	33	0.11	23.61
T2K(0) X 12340	10.09	3.84	0.95	16	0.10	34.02

(ΔRTT109::hph)						
T2k(0) X 12675(Δddi1::hph)	3.83	0.00	0.00	4	0.19	30.07
T2k(0) X 12414(Δmus-8::hph)	7.50	2.85	1.01	8	0.18	43.95
DLL-14-1 X 16329(Δdsk2::hph)	5.18	0.31	0.10	9	0.18	36.45
T2k(0) X 16857(ΔNACHT::hph)	4.97	0.54	0.20	7	0.24	46.73
DLL-14-1 X 11945(ΔNACHT::hph)	4.76	1.54	0.63	6	0.21	39.19
T2k(0) X 12532(ΔNACHT::hph)	4.67	0.78	0.45	3	0.23	36.66
DLL-14-1 X 13941(ΔNACHT::hph)	5.02	0.79	0.24	11	0.19	37.08
DLL-14-1 X 12862(ΔNACHT::hph)	5.13	0.00	0.00	2	0.15	30.57
DLL-14-1 X 12118(ΔNACHT::hph)	5.19	0.74	0.22	11	0.20	40.03
T2k(0) X 12338(ΔNACHT::hph)	5.93	0.84	0.32	7	0.21	44.30
T2k(0) X 11987(ΔNACHT::hph)	5.28	0.55	0.19	8	0.21	41.63
DLL-14-1 X 11270(ΔIDI-4::hph)	5.11	0.59	0.34	3	0.21	38.21
T2k(0) X 11925(Δmod-a::hph)	4.32	0.60	0.19	10	0.32	47.03
T2k(0) X 12377(Δmod-d::hph)	4.61	0.73	0.19	14	0.21	34.01
DLL-14-1 X 11868(ΔIDI-6::hph)	4.11	1.05	0.43	6	0.31	48.13
T2k(0) X 15891(ΔDCL-1::hph)	4.67	0.48	0.14	12	0.20	34.16
DLL-14-1 X 11155(ΔDCL-2::hph)	4.63	0.33	0.15	5	0.20	35.48
qde-2::unPA	4.67	2.92	0.56	27	n/a	40.00
DLL14-1 X 11101(Δbcl6::hph)	3.92	0.38	0.11	12	0.20	28.68
T2K(0) X 19554 ("ΔAID"::hph)	4.05	0.43	0.17	6	0.20	30.15
DLL14-1 X 20272("ΔAID"::hph)	5.77	0.36	0.12	9	0.18	39.29
DLL14-1 X 11347(Δbcl6::hph)	6.37	0.36	0.12	8	0.22	51.76
DLL14-1 X 11132(Δbcl6::hph)	5.34	1.13	0.35	10	0.18	36.27
DLL14-1 X 11344(Δbcl6::hph)	7.02	2.72	1.21	5	0.09	21.32

T2K(0) X 16008 (Δbcl6::hph)	5.88	0.93	0.35	7	0.22	43.74
T2K(0) X 15425 (Δbcl6::hph)	5.26	0.68	0.24	8	0.22	38.34
DLL14-1 X 11483(Δbcl6::hph)	5.88	1.09	0.41	7	0.18	33.81
DLL14(6) x DLL T5b (ΔBcl6 :: hph)	5.17	0.30	0.07	16	0.14	26.57
vib-1	24.00	n/a	0.00	0	0.85	80
DLL14(6) X 17936(ΔIme2::hph)	5.26	1.53	0.48	10	0.13	23.06
DLL14(6) X 12180 (ΔNdt80::hph)	3.43	0.84	0.25	11	0.31	34.99
DLL14-1 X 12529(ΔMSH2::hph)	3.49	0.50	0.13	14	0.21	27.38
T2K(0) X 12524(ΔMLH1::hph)	3.52	0.45	0.13	12	0.26	35.03
T2K(0) X 11970(ΔMLH1::hph)	3.2	0.25	0.08	8	0.22	27.65
T2k(0) X 15721(ΔTFB5::hph)	4.88	0.72	0.42	3	0.31	56.15
T2k(0) X 11189(ΔRad9::hph)	3.75	0.52	0.16	10	0.23	33.31
DLL-14-1 X 12053(ΔSnm1-like::hph)	4.85	0.82	0.27	9	0.19	36.12
DLL14-1 X 12530(ΔMLH3::hph)	4.31	0.50	0.14	12	0.26	39.91
T2k(0) X 18151(ΔESC2::hph)	3.63	0.40	0.09	16	0.30	34.05
DLL14(6) X 11914(Δhistone-lysine N-methyltransferase)	4.52	0.90	0.28	10	0.28	41.69
DLL14(6) X 18735(Δ hypothetical protein ::hph)	3.46	0.72	0.18	15	0.23	28.65
T2k(0) X 19786(Δ PIK1a::hph)	4.10	0.31	0.10	9	0.18	25.64
DLL14(6) X 11191(ΔRad1::hph)	3.88	1.38	0.30	20	0.18	24.17
DLL14(6) X 11548 (Δ phosphatase-Z-like-1 :: hph)	4.47	0.67	0.22	9	0.21	34.23
T2K(0) x 15739 (ΔULP2 :: hph)	4.47	0.67	0.22	9	0.19	29.43

Appendix C. All RT-qPCR values (threshold = 0.05).

Time (h)	0			1		2			5			8		
HU (mM)	0	80	120	0	80	0	80	120	0	80	120	0	80	120
vib-1	19.37	19.11	21.66	21.8	21.27	20	19.97	20.66	19.46	21.2	21.31	19.82	18.68	19.93
het-6	24.24	25.88	24.5	26.55	25.02	23.77	23.38	25.39	24.97	26.08	25.1	24.09	23.85	24.4
pin-c	26.57	26.58	25.09	25.98	30.89	26.39	27.07	28.38	27.15	25.32	25.93	26.18	24.69	25.04
tol	22.72	22.79	22.25	24.14	24.1	22.38	23.28	22.99	22.59	23.61	23.44	23.5	23.36	25.87
un-24	17.81	18.14	17.88	17.57	16.94	17.26	16.03	16.23	18.49	15.49	15.56	19.32	14.12	15.39
actin	14.27	13.83	14.42	13.44	14.72	13.6	13.37	12.78	14.25	14.2	14.31	13.88	14.26	13.97

References

Bartek, J. & Lucas, J. (2007). DNA damage checkpoints: from initiation to recovery or adaptation. *Curr. Opin, Cell Biol*, *19*, 238–245.

Belyi, V. A., Ak, P., Markert, E., Wang, H., Hu, W., Puzio-Kuter, A. & Levine, A. J. (2010). The origins and evolution of the *p53* family of genes. *Cold Spring Harbor perspectives in biology*, *2*(6), a001198.

Biella, S., Smith, M. L., Cortesi, P. & Milgroom, M. G. (2002). Programmed cell death correlates with virus transmission in a filamentous fungus. *Proceedings of the Royal Society of London B: Biological Sciences*, *269*(1506), 2269-2276.

Boiteux, S., & Jinks-Robertson, S. (2013). DNA repair mechanisms and the bypass of DNA damage in *Saccharomyces cerevisiae*. *Genetics*, *193*(4), 1025-1064.

Branzei, D. & Foiani, M. (2008). Regulation of DNA repair throughout the cell cycle. *Nat. Rev. Mol. Cell Biol, 9*, 297–308.

Buckland, R. J., Watt, D. L., Chittoor, B., Nilsson, A. K., Kunkel, T. A. & Chabes, A. (2014). Increased and imbalanced dNTP pools symmetrically promote both leading and lagging strand replication infidelity. *PLoS Genet*, *10*(12), e1004846.

Chandra, V., Bortnick, A., & Murre, C. (2015). AID targeting: old mysteries and new challenges. *Trends in Immunology*, *36*(9), 527-535.

Charlesworth, D., Vekemans, X., Castric, V. & Glémin, S. (2005). Plant self-incompatibility systems: a molecular evolutionary perspective. *New Phytologist*, *168*(1), 61-69.

Chevanne, D., Saupe, S. J., Clavé, C. & Paoletti, M. (2010). WD-repeat instability and diversification of the *Podospora anserina hnwd* non-self recognition gene family. *BMC evolutionary biology*, *10*(1), 134.

Ciccia, A. & Elledge, S. J. (2010). The DNA damage response: making it safe to play with knives. *Molecular cell*, *40*(2), 179-204.

Collins, D. W., & Jukes, T. H. (1994). Rates of transition and transversion in coding sequences since the human-rodent divergence. *Genomics*, *20*(3), 386-396.

Davis, R. H., & de Serres, F. J. (1970). Genetic and microbiological research techniques for *Neurospora crassa*. *Meth. Enzymol*, *17*, 79-143

Debets, A. J., & Griffiths, A. J. (1998). Polymorphism of *het*-genes prevents resource plundering in *Neurospora crassa*. *Mycological Research*, *102*(11), 1343-1349.

Debets, F., Yang, X., & Griffiths, A. J. (1994). Vegetative incompatibility in *Neurospora*: its effect on horizontal transfer of mitochondrial plasmids and senescence in natural populations. *Current genetics*, *26*(2), 113-119.

Dementhon, K., Iyer, G., & Glass, N.L. (2006). VIB-1 is required for expression of genes necessary for programmed cell death in *Neurospora crassa. Eukaryot. Cell*, 5, 2161–2173.

Espagne, E., Balhadère, P., Penin, M. L., Barreau, C., & Turcq, B. (2002). HET-E and HET-D belong to a new subfamily of WD40 proteins involved in vegetative incompatibility specificity in the fungus *Podospora anserina*. *Genetics*, *161*(1), 71-81.

Glass, N.L., Jacobson, D.J., & Shiu, P.K. (2000). The genetics of hyphal fusion and vegetative incompatibility in filamentous ascomycete fungi. *Annu Rev Genet*, *34*, 165-186.

Gray, S., Allison, R. M., Garcia, V., Goldman, A. S., & Neale, M. J. (2013). Positive regulation of meiotic DNA double-strand break formation by activation of the DNA damage checkpoint kinase Mec1 (ATR). *Open biology*, *3*(7), 130019.

Hall, C., Welch, J., Kowbel, D. J., & Glass, N. L. (2010). Evolution and diversity of a fungal self/nonself recognition locus. *PLoS One*, *5*(11), e14055.

Hepworth, S. R., Friesen, H., & Segall, J. (1998). *NDT80* and the meiotic recombination checkpoint regulate expression of middle sporulation-specific genes in *Saccharomyces cerevisiae*. *Molecular and Cellular Biology*, *18*(10), 5750–5761.

Jordan, A., & Reichard, P. (1998). Ribonuleotide reductases. *Annu Rev Biochem*, *67*, 71-98.

Kaneko, I., Dementhon, K., Xiang, Q., & Glass, N. L. (2006). Nonallelic interactions between *het-c* and a polymorphic locus, *pin-c*, are essential for nonself recognition and programmed cell death in *Neurospora crassa*. *Genetics*, *172*(3), 1545-1555.

Kazama, Y., Ishii, C., Schroeder, A. L., Shimada, H., Wakabayashi, M., & Inoue, H. (2008). The *Neurospora crassa* UVS-3 epistasis group encodes homologues of the ATR/ATRIP checkpoint control system. *DNA repair*, *7*(2), 213-229.

Krakoff, I. H., Brown, N. C., & Reichard, P. (1968). Inhibition of ribonucleoside diphosphate reductase by hydroxyurea. *Cancer Research*, *28*(8), 1559-1565.

Kumanovics, A., Takada, T., & K.F. Lindahl. (2003). Genomic organization of the mammalian MHC. *Annu Rev Immunol., 21*, 629-57.

Lafontaine, D. L., & Smith, M. L. (2012). Diverse interactions mediate asymmetric incompatibility by the *het-6* supergene complex in *Neurospora crassa*. *Fungal Genetics and Biology*, *49*(1), 65-73.

Lafontaine, D.L. (2010). Genetic and epigenetic of a nonself recognition complex in *N. crassa*. MSc thesis. Carleton University.

Lavin, M. F., Kozlov, S., Gatei, M., & Kijas, A. W. (2015). ATM-Dependent Phosphorylation of All Three Members of the MRN Complex: From Sensor to Adaptor. *Biomolecules*, *5*(4), 2877-2902.

Lieber, M. R. (2010). The mechanism of double-strand DNA break repair by the nonhomologueous DNA end joining pathway. *Annual review of biochemistry*, *79*, 181.

Leslie, J.F., & Yamashiro, C.T. (1997). Effects of the *tol* mutation on allelic interactions at *het* loci in *Neurospora crassa*. *Genome*, *40*(6), 834-840.

Liu, M., Duke, J.L., Richter, D.J., Vinuesa, C.G., Goodnow, C.C., Kleinstein, S.H., & Schatz, D.G. (2008). Two levels of protection for the B cell genome during somatic hypermutation. *Nature*, *451*, 841–845.

Livak, K. J., & Schmittgen, T. D. (2001). Analysis of relative gene expression data using real-time quantitative PCR and the 2− ΔΔCT method. *methods*, *25*(4), 402-408.

MacLennan, I.C. (1994). Germinal centers. *Annu. Rev. Immunol*.,*12*, 117–139.

Majka, J., Niedziela-Majka, A., & Burgers, P. M. (2006). The checkpoint clamp activates Mec1 kinase during initiation of the DNA damage checkpoint. *Molecular cell*, *24*(6), 891-901.

Mantovani, F., Zannini, A., Rustighi, A., & Del Sal, G. (2015). Interaction of *p53* with prolyl isomerases: Healthy and unhealthy relationships. *Biochimica et Biophysica Acta (BBA)-General Subjects*, *1850*(10), 2048-2060.

Maréchal, A., & Zou, L. (2013). DNA damage sensing by the ATM and ATR kinases. *Cold Spring Harbor perspectives in biology*, *5*(9), a012716.

Micali, O.C., & Smith, M.L. (2006). A nonself recognition complex in *Neurospora crassa*. *Genetics*, *173*, 1991-2004.

Miller, M. B., & Bassler, B. L. (2001). Quorum sensing in bacteria. *Annual Reviews in Microbiology*, *55*(1), 165-199.

Mir-Rashed, N., Jacobson, D.J. Dehghani, M.R., Micali, O.C. & Smith, M.L. (2000). Incompatibility genes at *het-6* as genetic markers in a population of *Neurospora crassa*. *Fungal Genet. Biol.,* 30, 197-205.

Nasrallah, J. B. (2002). Recognition and rejection of self in plant reproduction. *Science*, *296*(5566), 305-308.

Nasrallah, J. B. (2005). Recognition and rejection of self in plant self-incompatibility: comparisons to animal histocompatibility. *Trends in immunology*, *26*(8), 412-418.

Newmeyer, D., & Galeazzi, D. R. (1978). A meiotic UV-sensitive mutant that causes deletion of duplications in *Neurospora*. *Genetics*, *89*(2), 245-269.

Perkins, D. D. (1986). Hints and precautions for the care, feeding and breeding of *Neurospora*. *Fungal Genet. Newslett, 33*, 35-41.

Pittenger, T.H. (1964). Spontaneous alteration of heterokaryon compatibility factors in *Neurospora*. *Genetics*, *50*, 471-484.

Raju, N. B. (1982). Easy methods for fluorescent staining of Neurospora nuclei. *Neurospora Newsl*, *29*, 24-26.

Ranuncolo, S.M., Polo, J.M., & Melnick, A. (2008). BCL6 represses CHEK1 and suppresses DNA damage pathways in normal and malignant B-cells. *YBCMD*, *41*, 95-99.

Reichard, P. (2001). Ribonucleotide reductases: the evolution of allosteric regulation. *Arch. Biochem. Biophys, 397,* 149-155

Reshke, R. (2013). Developing a catalytically functional ribonucleotide reductase for *Neurospora crassa* that lacks heterokaryon incompatibility activity. MSc thesis. Carleton University.

Reuter, K., Steinbach, A., & Helms, V. (2016). Interfering with Bacterial Quorum Sensing. *Perspectives in Medicinal Chemistry*, *2016*(8), 1-15.

Sanchez, Y., Desany, B. A., Jones, W. J., Liu, Q., Wang, B., & Elledge, S. J. (1996). Regulation of RAD53 by the ATM-like kinases MEC1 and TEL1 in yeast cell cycle checkpoint pathways. *Science*, *271*(5247), 357-360.

Schroeder, A. L. (1970). Ultraviolet-sensitive mutants of Neurospora. *Molecular and General Genetics MGG*, *107*(4), 291-304.

Schroeder, A. L. (1986). Chromosome instability in mutagen sensitive mutations of *Neurospora crassa*. *Curr. Genet., 10*, 381-388.

Smith, R. P., Wellman, K., Haidari, L., Masuda, H., & Smith, M. L. (2013). Nonself recognition through intermolecular disulfide bond formation of ribonucleotide reductase in *Neurospora*. *Genetics, 193*, 1175-1183.

Smith, M. L., & Lafontaine, D. L. (2012). The fungal sense of nonself. In: *Neurospora* Genomics and Molecular Biology. Eds. Kevin McCluskey and D. Kasbekar, Horizon Scientific Press, Norfolk UK.

Smith, M.L., Micali, O.C., Hubbard, S.P., Mir-Rashed, N., Jacobson, D.J. , & Glass, N.L. (2000). Vegetative incompatibility in the *het-6* region of *Neuospora crassa* is mediated by two linked genes. *Genetics*, *155*, 1095-1104.

Smith, M.L., Yang, C.J., Mehenberg, R.L., & Glass, N.L. (1996). Escape from *het-6* incompatibility in *Neurospora crassa* partial diploids involves preferential deletion within the ectopic segment. *Genetics, 144*, 523-531.

Tock, M. R., & Dryden, D. T. (2005). The biology of restriction and anti-restriction. *Current opinion in microbiology*, *8*(4), 466-472.

Vellani, T.S., Griffiths, A.J., & Glass N.L. (1994). New mutations that suppress mating-type vegetative incompatibility in *Neurospora crassa*. *Genome*, *37*(2), 249-255.

Wakabayashi, M., Ishii, C., Inoue, H., & Tanaka, S. (2008). Genetic analysis of CHK1 and CHK2 homologues revealed a unique cross talk between ATM and ATR pathways in Neurospora crassa. *DNA repair*, *7*(12), 1951-1961.

Watanabe, K., Sakuraba, Y., & Inoue, H. (1997). Genetic and molecular characterization of Neurospora crassamus-23: a gene involved in recombinational repair. *Molecular and General Genetics MGG*, *256*(4), 436-445.

Xiang, Q., & Glass, N.L. (2002). Identification of *vib-1*, a locus involved in vegetative incompatibility mediated by *het-c* in *Neurospora crassa*. *Genetics*, *162*, 89–101.

Xiang, Q., & Glass, N.L. (2004). The control of mating type heterokaryon incompatibility by *vib-1,* a locus involved in het-c heterokaryon incompatibility in *Neurospora crassa. Fungal Genet. Biol, 41*, 1063–1076

Xu, L., Ajimura, M., Padmore, R., Klein, C., & Kleckner, N. (1995). NDT80, a meiosis-specific gene required for exit from pachytene in *Saccharomyces cerevisiae. Mol Cell Biol, 15*(12), 6572-6581.

Zan, H., & Casali, P. (2015). Epigenetics of Peripheral B-Cell Differentiation and the Antibody Response. *Frontiers in immunology*, *6*.

Zeman, M. K., & Cimprich, K. A. (2014). Causes and consequences of replication stress. *Nature cell biology*, *16*(1), 2-9.

Zhang, Z., Yang, Q., Sun, G., Chen, S., He, Q., Li, S., & Liu, Y. (2014). Histone H3K56 acetylation is required for quelling-induced small RNA production through its role in homologous recombination. *Journal of Biological Chemistry*, *289*(13), 9365-9371.

Zou, L. (2013). Four pillars of the S-phase checkpoint. *GenesDev, 27*, 227-233.